Materials Horizons

ROYAL SOCIETY OF CHEMISTRY

REVIEW

View Article Online
View Journal

Cite this: DOI: 10.1039/d5mh01692d

Stochastic dynamics of nanoparticle catalysis: a discrete-state perspective

Pankaj Jangid and Srabanti Chaudhury *

Received 5th September 2025,
Accepted 2nd December 2025

DOI: 10.1039/d5mh01692d

rsc.li/materials-horizons

Recent advancements in single-molecule techniques have allowed researchers to investigate individual nanocatalysts, which exhibit inherent variations in size, shape, and surface properties, leading to unique and time-dependent catalytic behaviors. The heterogeneity in surface facets, defects, and structural dynamics further influences their performance, highlighting the importance of single-particle analysis in catalyst development. Recent theoretical studies using stochastic modeling have provided valuable insights into the microscopic dynamics of nanoparticle catalysis. This review systematically examines the impact of active site heterogeneity on reaction dynamics, the role of dynamic catalytic restructuring in enhancing efficiency, and the emergence of intra-particle catalytic cooperativity through charged hole dynamics. By integrating these theoretical advances, this review offers a comprehensive perspective on the microscopic mechanisms governing nanoparticle catalysis and suggests potential avenues for the rational design and understanding of more effective catalytic systems.

Wider impact

Understanding the underlying chemical and physical mechanisms of a catalyst at the single-particle level opens new ways for efficient catalyst design. Theoretical models and numerical simulations have proven valuable in providing both quantitative and qualitative insights into catalyst dynamics. Stochastic methods are useful for moving beyond the bulk measurements and uncovering the complexity of nanocatalyst behavior. This review gathers recent theoretical studies using stochastic modeling to show how intrinsic fluctuations and heterogeneity influence the reaction dynamics of nanocatalysts. The key developments discussed include the application of theoretical models to resolve heterogeneity in size, shape, and surface facets, stochastic models that connect microscopic active-site fluctuations to macroscopic kinetics, and the identification of the role of dynamic restructuring and charged hole-mediated cooperativity as drivers of enhanced and time-dependent catalytic activity. This area is of broad interest in catalysis modeling, as moving beyond ensemble averages uncovers mechanistic complexity that reveals catalyst performance and selectivity, which are central to sustainable energy conversion and green synthesis. Furthermore, integrating real-time single-particle experiments with stochastic and data-driven models will enable the development of atomically informed design rules for next-generation catalysts.

1 Introduction

Heterogeneous catalysts can accelerate chemical reactions with high selectivity and are proven to be vital in industrial processes. They play a critical role in shaping our society and will be essential for its sustainable future.[1] The catalysts must be highly efficient and environmentally friendly for this role. The design and development of new catalysts have been heavily based on traditional trial-and-error experimental methods.[2] Several theoretical and computational studies at different scales of investigation have become a reasonable choice in the initial design and understanding of catalysts.[3,4]

Nanoparticle catalysts have revolutionized heterogeneous catalysis due to their unique size- and shape-dependent properties and high surface area and the ability to tailor their surface characteristics through simple modifications.[5,6] These catalysts are highly complex materials optimized for use with high selectivity and reaction rates. The composition and structure of these catalysts can be tuned to obtain high performance under the given reaction conditions.[7–10] Nanocatalysts have been known for more than a century and have been studied by many experimental and theoretical methods. Advances in single-molecule techniques have enabled researchers to discover new results that existing theoretical studies could not achieve.[11–16]

Single-molecule fluorescence microscopy experiments have been able to investigate chemical reactions on nanocatalysts. These experiments can provide insight into the catalyst behavior with unprecedented spatial and temporal resolutions that have revealed multiple new features.[17–23] Individual nanocatalysts differ in size, shape, and surface sites, leading to

Department of Chemistry, Indian Institute of Science Education and Research, Pune, 411008, India. E-mail: srabanti@iiserpune.ac.in; Tel: +91 2025908140

time-dependent, particle-specific catalytic activity.[24–32] Surface facets and surface defects can affect the catalytic activity. Active site heterogeneity has been observed by several density functional theory (DFT) studies as well.[33–36] Catalysts can also undergo structural changes under reaction conditions, leading to fluctuations in temporal activity and coverage fluctuations that also differ from one nanoparticle to another.[37–41] Smaller nanoparticles, often called nanoclusters, can undergo isomerization due to thermal fluctuations, where several different forms with different catalytic activities can be present.[42–46] This leads to temporal heterogeneity in their catalytic dynamics. The development of *in situ* and operando techniques has become critically important because they enable observation under reaction conditions while providing structural, morphological, compositional, and chemical state information in working environments.[26,47–57] These techniques have also advanced our understanding of dynamic active-site transformations.[37,58,59] Experimental studies have also suggested the existence of spatial communication between different active sites within a single nanocatalyst[60,61] and single atom catalysts.[62,63] These findings highlight that nanocatalysts can exist in dynamically evolving structural states, exhibiting spatial and temporal variations in their catalytic properties.

Computational techniques and mathematical modeling have been widely used to study complex dynamical systems, including biochemical networks and complex cellular processes.[64,65] Although there are numerous theoretical models in the literature to study nanoparticle catalysts, many of them are based primarily on bulk properties and assumptions derived from conventional heterogeneous catalysis.[66–68]

Mathematical modeling of chemical systems heavily relies on deterministic mass action kinetics, where the dynamical evolution of reactants and products is given by ordinary differential equations.[4,69,70] The deterministic methods generally assume macroscopic concentrations and spatial homogeneity in the system, which effectively averages out fluctuations at the molecular level. For systems at the nanoscale level with a low molecular number, this averaging is no longer valid. Single-molecule experimental techniques treat catalytic turnover as a sequence of discrete reaction events that occur at an individual active site.[29,71,72] The observed catalytic dynamics in such experiments are noisy processes, where the intrinsic fluctuations may affect the stationary and transient behavior both qualitatively and quantitatively. In systems where the number of molecules is small and discrete, intrinsic noise is not merely a perturbation. In such cases, the predictions of stochastic and deterministic approaches can significantly differ and produce distinct steady states.[73,74] Another disadvantage of deterministic methods is that the assumption of mean-field kinetics is not applicable to heterogeneous nanoparticles with multiple types of sites, varying particle shapes, and sizes, which are challenging to assess.[25,71,75] As a result, deterministic models may predict behaviour that significantly differs from experimental observation in real nanoscale systems. The small size of catalysts results in discrete coverages of adsorbate molecules, which is difficult to describe using a mean-field model.[76]

To account for molecular fluctuations, where the number of key species is low and stochasticity plays a determining role in system dynamics, stochastic approaches are required. The stochastic counterparts of chemical kinetics, such as the chemical master equation (CME), can explicitly describe the probabilistic nature of reaction events in small systems.[77,78] Computer simulation techniques such as Gillespie's algorithm and kinetic Monte Carlo (KMC) can sample several individual reaction trajectories. Such techniques can directly model discrete molecular interactions and capture behaviors driven by noise.[79–82]

In this review, we restrict our focus on the mathematical models rather than the variety of experimental techniques and software tools used in heterogeneous catalysis. Mathematical models evaluate the microscopic interplay between elementary processes in a catalytic system. We critically examine the physical foundations of the catalyst at the molecular level, the validity of the presented mathematical models, and the underlying assumptions.

2 Techniques to study catalysis

2.1 Chemical master equation

For long-time evolution (on the order of thousands of turnover events), a catalytic system can be assumed to involve transitions between minimum energy states of the potential energy surface. The system exists in the minimum energy state for a sufficiently long time before jumping into the next state, so it forgets about the past state from which it came. A process with state-to-state memoryless jumps can describe such dynamics, also called the Markovian dynamics.[77] A widely used method for analyzing systems with jump processes and inherent stochasticity is the CME.[77,83] Unlike the deterministic kinetic equations, where a deterministic differential equation gives the time evolution of the number of reaction species, the CME gives the time evolution of the probability of the number of reaction species. One of the key advantages of the CME framework is its ability to generate the full probability distribution of events, rather than just their average values. Generally, the mean predicted by the CME converges to the quantities obtained from ensemble-based approaches. The CME is a versatile tool that can be used in various fields to model jump processes.[84] A schematic representation of jump processes is given in Fig. 1(a), where each discrete state can be considered as a specific configuration of reactants and products on the catalyst surface, lower panel in Fig. 1(a). Two different configurations or numbers of reaction species correspond to two different discrete states.

Suppose a chemical reaction consists of M chemical species that can be present in N distinct chemical states. A chemical state, $n = (n_1, n_2, \ldots, n_M)$, can be considered a vector that indicates the number of different reaction species. Note that the specific arrangement of different reaction species on the surface is ignored here. However, for a detailed description of the system, the chemical state n also consists of specific locations and orientations of reactants, see Fig. 1(b). The

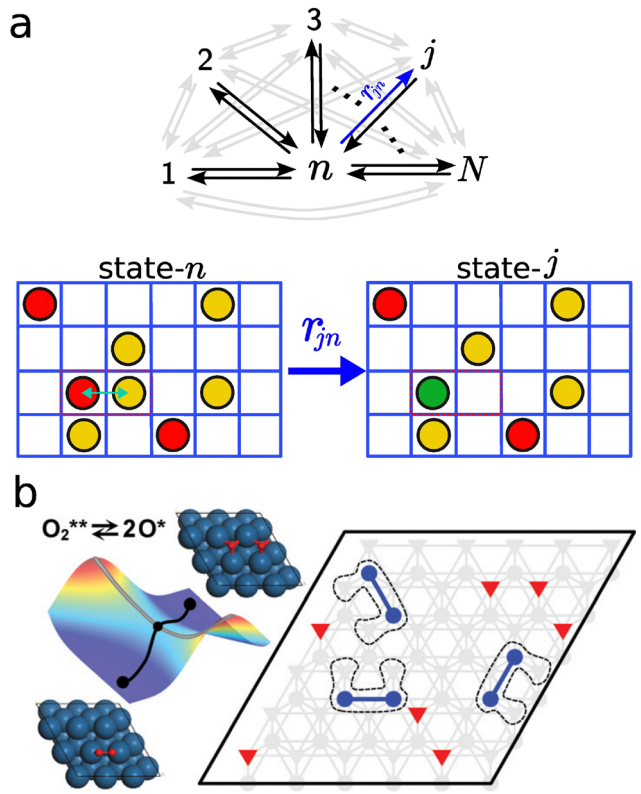

Fig. 1 (a) Schematic diagram of a network of N discrete states. A discrete state is a coarse grained version of a long lived catalytic state where each discrete state can be a specific configuration of microstates of the catalyst. (b) Schematic of O_2 dissociation on a catalytic surface where different orientations of the adsorption can also represent different discrete states. Panel (b) is reproduced with permission from ref. 82, Copyright 2012 American Chemical Society.

reaction can be in any of the N chemical states at any instant. The transition rate from state i to state j is defined as r_{ji}. Let $P(n,t|n_0,t_0)$ be the probability density function for finding the system in state n, since the system was in state n_0 at some earlier time t_0. Then the time evolution of $P(n,t|n_0,t_0)$ can be written using the forward CME

$$\frac{\mathrm{d}P(n,t|n_0,t_0)}{\mathrm{d}t} = \sum_{\substack{j=0 \\ j\neq n}}^{N} \left[r_{nj}P(j,t|n_0,t_0) - r_{jn}P(n,t|n_0,t_0)\right] \quad (1)$$

Here, the first term in the summation on the right-hand side indicates the gain in probability, and the second term indicates the loss in probability. Using eqn (1), the probability distribution can be calculated. For clarity, we will remove the initial conditions in the probability densities and write $P(n,t)$. Let $P(n)$ denote the steady state distribution of state n, which is defined as $P(n) = P(n,t \to \infty)$. Therefore, from the forward CME, we can write

$$\sum_{\substack{j=0 \\ j\neq n}}^{N} \left[r_{nj}P(j) - r_{jn}P(n)\right] = 0 \quad (2)$$

The forward CME has been used in several studies, making it a versatile tool in various disciplines. In the CME equation (eqn (1)), the waiting time distribution before making a transition is exponentially distributed. However, when the waiting-time distribution deviates from a single exponential, a more general form of master equations can be used.[83,85]

2.2 First passage time

In catalysis, we are generally interested in the time it takes for the reactants to form the products. The time taken by any stochastic process from an initial state to a final state for the first time is known as the first passage time (FPT).[77,83,86] It is also called the first hitting time and exit time in the literature. The time evolution of the FPT probability density function is governed by a backward CME. Suppose a process starts from an initial state n at time t_0 and reaches a fixed state m at time t', for the first time. The backward CME describes how the probability density changes as a function of the initial state n, keeping the final state m fixed. It evolves the probability backward, which is written as[77]

$$\frac{\mathrm{d}P(m,t'|n,t_0)}{\mathrm{d}t_0} = \sum_{\substack{j=0 \\ j\neq m}}^{N} \left[r_{jm}P(m,t'|n,t_0) - r_{jm}P(m,t'|j,t_0)\right]. \quad (3)$$

In the backward CME, the final state is absorbing, which means $P(m,t'|m,t_0) = \delta(t - t_0)$. This indicates that if we start the process from the final state, it will be instantly achieved. For clarity, the FPT probability density can be written in a different form keeping only initial conditions, $F(n,t) = P(m,t'|n,t_0)$ and $F(j,t) = P(m,t'|j,t_0)$, where $t = t' - t_0$ is the time taken to achieve the final state. Then the backward CME in eqn (3) reads

$$\frac{\mathrm{d}F(n,t)}{\mathrm{d}t} = \sum_{\substack{j=0 \\ j\neq n}}^{N} \left[r_{jn}F(j,t) - r_{jn}F(n,t)\right]. \quad (4)$$

In a stochastic process, several trajectories are possible from the initial to the final state, and the time taken in those trajectories (FPT) is a random variable. Therefore, a statistical approach is used to realize several first passage times, and the mean and higher moments of FPT can be obtained.

The backward master equation offers several advantages, particularly in problems that focus on how future outcomes depend on the initial state. It is especially well-suited for calculating quantities like the mean first-passage time (MFPT) and survival and absorption probabilities. Note that the same problems can be solved by the forward CME by applying suitable boundary and initial conditions.[77] Unlike the forward equation, which evolves the full probability distribution over time, the backward equation allows one to isolate the role of the starting point and simplifies the analysis of stochastic processes where the path to a target or an absorbing state is of primary interest.[77] Using $F(n,t)$ the moments of FPT can be obtained using simple probability theory rules of

expectation value.

$$\langle \tau^r \rangle = \int_0^\infty t^r F(n,t)\mathrm{d}t \tag{5}$$

Generally, it is difficult to solve for the full FPT distribution in the time domain. However, it is easier to solve the first-order differential equation in Laplace space, where the differential equation becomes a simple linear algebraic equation.[84] Let the Laplace transform of $F(n,t)$ be written as $\tilde{F}(n,s) = \int_0^\infty \mathrm{e}^{-st}F(n,t)\mathrm{d}t$. Then the rth moment of the first passage time can be written as

$$\langle \tau^r \rangle = (-1)^r \frac{\mathrm{d}^r \tilde{F}(n,s)}{\mathrm{d}s^r}\bigg|_{s=0}. \tag{6}$$

2.3 Stochastic fluctuation quantification

Catalytic turnover from a single nanoparticle is intrinsically noisy and physically relevant information is concealed in the noise, emphasizing the importance of stochastic fluctuations in observable quantities. Several studies have shown the importance of stochastic effects in biological systems such as living cells,[87,88] physical phenomena such as phase transitions,[89] chemical kinetics, and nanocatalysts.[14,71] In the ensemble experiments, the stochastic fluctuations are often averaged out. Stochastic modeling methods allow us to estimate the higher moments of turnover times from nanocatalysts, which can provide valuable information on the nature of fluctuations. Several statistical parameters are used in the literature for this purpose, such as the Fano factor, Poisson indicator, coefficient of variation, and randomness parameter.[90–95] These parameters are based on the first and second moments of observable quantities, which are used to probe the extent of stochastic fluctuations in the system. In single-molecule turnover reactions, the quantification of stochasticity is generally done using a statistical quantity known as the randomness parameter, R.[93–98] It is defined as

$$R = \frac{\langle \tau^2 \rangle - \langle \tau \rangle^2}{\langle \tau \rangle^2} = \frac{\mathrm{Var}(\tau)}{\langle \tau \rangle^2}. \tag{7}$$

Single molecule experiments provide the distribution of the individual product formation event. Randomness can be easily calculated from single turnover statistics from these experiments. For a single-step Poisson process, the waiting time distribution is exponential and the numerical value of R will be unity. If there are multiple rate-determining kinetic processes, the distribution becomes nonexponential, and R deviates from unity. In the case of multiple rate-limiting steps, the waiting time distribution has a peak followed by decay, and the randomness parameter will be less than one. If the distribution has long multiexponential tails, it indicates that there are multiple parallel pathways to reach the product and one observes $R > 1$. Thus R provides a quantitative idea of the shape of the dwell time distribution. It measures the degree of stochastic fluctuations and provides information on the underlying chemical kinetic scheme. Deviation in the value of R from unity is a manifestation of the dynamic disorder. Earlier studies indicated that R provides information about the number of steps (intermediates) present in a stochastic system. The reciprocal of R gives the bound for the number of rate-limiting states for sequential kinetic schemes. Therefore, different values of R can hint at hidden states, multiple rate-limiting steps, dynamic disorder, off-pathway branches, and non-exponential statistics.[93,94]

We take an example of a simple reaction with irreversible steps n, each with the same rate constant.

$$A_1 \xrightarrow{k} A_2 \xrightarrow{k} A_3 \xrightarrow{k} \cdots \xrightarrow{k} A_{n-1} \xrightarrow{k} A_n$$

The first passage time distribution of reaching A_n from A_1 in this case is a single exponential given by

$$F(t) = \frac{k^n \mathrm{e}^{-kt} t^{n-1}}{(n-1)!}. \tag{8}$$

Then, the MFPT and the second moment can be given by $\langle t \rangle = \int_0^\infty tF(t)\mathrm{d}t = n/k$ and $\langle t^2 \rangle = \int_0^\infty t^2 F(t)\mathrm{d}t = \frac{n(n+1)}{k^2}$. In this case, the randomness parameter is $R = 1/n$, which is the inverse of the number of steps in the reaction, and the number of rate-limiting steps in the dynamics can be estimated from the value of $1/R$. The value of R is important for the quantitative assessment of the microscopic mechanism. However qualitative trends of R can also be very informative.

2.4 Kinetic Monte Carlo simulations of nanoparticle catalysis

Kinetic Monte Carlo (KMC) is a powerful computational method to simulate reaction systems while considering intrinsic noise.[79,80] The KMC method is also known as Gillespie's Stochastic Simulation Algorithm (SSA). The KMC method is well-suited for chemical processes where the system evolves through discrete states with known transition rates. KMC can capture the correct temporal dynamics of rare events by sampling both the type and timing of the next reaction event. Extensions of the KMC algorithm for time-dependent rates and non-Markovian systems have also been proposed.[99–101]

One of the essential steps in the KMC simulation for real catalytic systems is the estimation of rate constants. Many studies use approximate values of rate constants based on fitting simple models to experimental data, approximating rates from similar known systems and statistical methods.[70,102–104] A more accurate and systematic approach is to utilize first-principles calculations and statistical methods to obtain rate parameters.[105–112] In the general framework of KMC, the system is described by a set of discrete states, each associated with a set of possible transitions characterized by reaction propensities.[113] The essential structure of this discrete event simulation algorithm is as follows:

1. Initialize the system: initialize the counts of all reaction species and set the simulation time to zero:

$$t = 0$$

2. Calculate the rates: for all possible transitions, i, from the current state calculate the rate (or propensity) k_i for each event and calculate the total rate, k_{tot} of transitions.

$$k_{tot} = \sum_i k_i$$

3. Calculate the next reaction time: draw a uniform random number r_1 from the interval (0,1) and calculate the time increment using

$$\Delta t = -\frac{\ln(r_1)}{k_{tot}}$$

and update the simulation time:

$$t \leftarrow t + \Delta t$$

4. Calculate the next reaction: draw a uniform random number r_2 from the interval (0,1). Determine the next event j by finding the smallest number j such that

$$\sum_{i=1}^{j} k_i > r_2 k_{tot} \geq \sum_{i=1}^{j-1} k_i$$

5. Update the system: according to the transition j in step 4 update the system state.

6. Repeat: store the updated state and simulation time for analysis and repeat steps 1–5 until the simulation does not reach the desired time, *e.g.* $t < t_{final}$.

From a simple one-step reaction to a highly complex surface catalyst dynamics, the scheme mentioned above remains at the heart of their stochastic simulations. The possible orientations of the reactant molecules can be accounted for in the KMC approach. Also, the KMC simulation facilitates modeling adsorption, desorption, and diffusion of reaction species while accounting for the shape and size of the nanocatalyst.[114–116] Studying heterogeneous catalysis with KMC simulations is a large and fast growing field. Interested readers can explore the detailed procedure reviewed here,[81,117,118] along with various software tools.[119–121]

3 Single molecule measurements in catalysis

Observations from single-molecule techniques have been well known in the case of enzyme catalysts. Single-molecule fluorescence microscopy is an indispensable tool in single-molecule studies that allow researchers to observe the behavior of individual molecules in real time.[122,123] These techniques provide a high signal-to-noise ratio for visualization while retaining key features in the physiological context of native biological systems. This approach was initially developed to study catalysis by single enzyme molecules.[124–127] The pioneering works on the enzyme catalysts and advancements in microscopy techniques have made it possible to probe the nanocatalysts at high spatial resolution.[13–15,71,128–130] By utilizing fluorogenic catalytic reactions and imaging the fluorescence signal of the product, one can monitor these reactions in real time at single-turnover resolution under steady-state reaction kinetics on a single nanoparticle.[14,71,131]

In the chemical reaction involved in single-molecule techniques, a non-fluorescent substrate (resazurin) gets converted to a fluorescent product (resorufin) on the nanoparticle surface.[14,15,71] Each product formation event results in a fluorescence burst when excited by a laser, which can be captured using fluorescence microscopy. Though the fluorescence burst in these reactions is very quick, the waiting time between two successive bursts, $\langle \tau_{off} \rangle$, is significant and can be detected with high temporal resolution. Similar techniques have been applied in the electrocatalysis at single-reaction resolution.[16]

Ensemble-averaged techniques such as the Langmuir–Hinshelwood mechanism, among others, were commonly employed to investigate nanoparticle catalysis theoretically.[14,71] These approaches are inspired by pioneering studies in enzymatic catalysis, where substrate binding and unbinding to the enzyme are treated as reversible processes.

Let a substrate S bind to the any one of the N active sites on a gold nanocatalyst surface, forming the bound state Au–S, which can form the product with rate k_2 as shown in the reaction mechanism in Fig. 2(a). Then the fraction of coverage of sites, the sites in Au–S states, in the limiting case where $k_2 \ll k_1$ and $k_2 \ll k_{-1}$ is given by

$$\theta = \frac{K[S]}{1 + K[S]} \quad (9)$$

where $K = k_1/k_{-1}$ is the equilibrium constant and [S] is the substrate concentration. Then the inverse of the waiting time before a fluorescence burst can be written as[71]

$$\langle \tau_{off} \rangle^{-1} = \frac{kNK[S]}{1 + K[S]} \quad (10)$$

Experimental data of $\langle \tau_{off} \rangle^{-1}$ for varied substrate concentrations and different sizes of the Au-nanoparticle catalyst are shown in Fig. 2(b), where the lines show fitting of eqn (10). With increasing substrate concentration, the Au-nanoparticles show a similar kinetics of $\langle \tau_{off} \rangle^{-1}$ as in eqn (10), solid fitted lines in Fig. 2(b). These observations can be well explained by the Langmuir–Hinshelwood approach.

4 Why stochastic modeling?

Microkinetic modeling, stochastic methods, and energy-landscape theory offer complementary but fundamentally distinct insights into catalytic phenomena. Microkinetic modeling employs a deterministic and mean-field approach, built from elementary reaction steps. This method is helpful for quantifying steady-state rates and identifying rate-determining steps in chemical reactions.[4,132,133] The use of a mean-field approximation and a heavy reliance on accurately known kinetic parameters limit its ability to capture the spatial and temporal

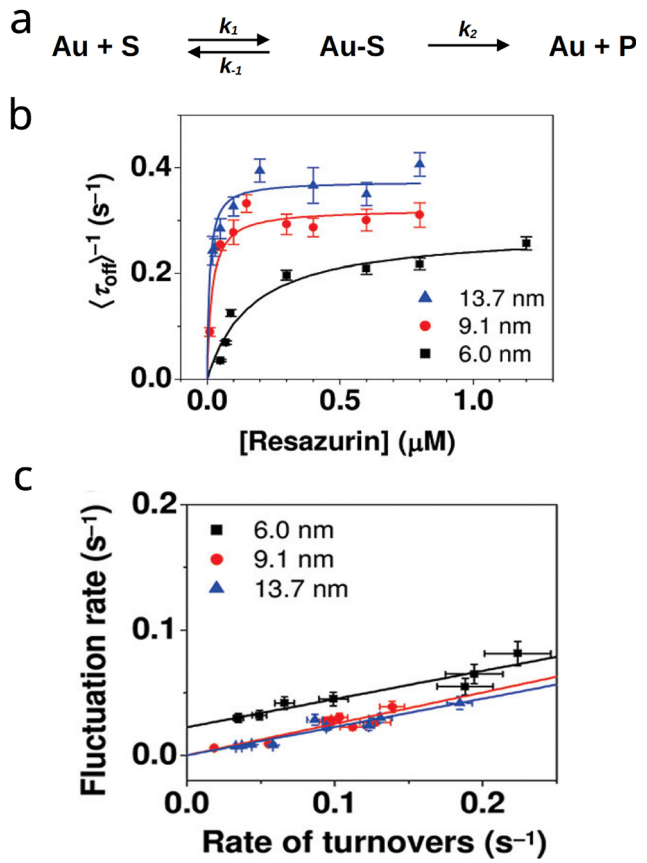

Fig. 2 (a) Michaelis–Menten chemical reaction for nanocatalysis. (b) Mean turnover rate as a function of substrate concentration for Au-nanoparticles of different sizes. (c) Activity fluctuation rate in the turnovers from the Au-nanocatalyst. (b) and (c) are reproduced with permission from ref. 14. Copyright 2009 American Chemical Society.

heterogeneity inherent in real nanocatalysts. Energy-landscape theory adopts a thermodynamic viewpoint and reveals design principles, such as the relationship between energy gaps and catalytic turnovers, while unifying kinetics and thermodynamics.[134–136] Stochastic models resolve catalysis at the level of individual nanoparticles or active sites, capturing microscopic heterogeneity and temporal fluctuations that ensemble approaches average out. Stochastic models provide direct access to turnover-time distributions, dynamic disorder, and rare events, which makes them highly valuable for interpreting data from single-particle spectroscopy and elucidating particle-to-particle variability.[91,95,98,137] However, their analytical intractability, high computational cost, and data requirements limit their use to nanoscale systems rather than large-scale systems. In short, stochastic methods can reveal microscopic heterogeneity, microkinetics quantitatively predict macroscopic rates and selectivity, and landscape theory provides generalizable design rules rooted in fundamental thermodynamics.

Since each turnover event in a single molecule experiment gives a different turnover time and activity fluctuation rate, this provides a measure to quantify the fluctuations in turnover. Fluctuations in activities can also arise due to dynamic restructuring.[14] Fig. 2(c) presents the fluctuation rate as a function of the turnover rate of the Au nanoparticles. This figure shows that the fluctuation rate is higher when the turnover rate is larger and the catalyst size is smaller. The Langmuir–Hinshelwood model presented in the previous section is based on the assumption that the Au catalyst surface is uniform and the substrate binding–unbinding reaction is very fast (compared to the product formation) and reaches equilibrium on the surface with a large area. However, if the number of catalytic sites is small, the average coverage approach does not work well as the θ will be a highly fluctuating random variable. In the analysis of individual reactions, higher moments of observables, generally the second moment, are vital in the statistical analysis. The ensemble approaches cannot produce such higher moments. Therefore, quantification of fluctuations requires stochastic methods that utilize the probabilistic approach to explain and predict the properties of reactions on nanoparticles while accounting for intrinsic fluctuations.[95] These methods become essential when the dynamics of catalysis is too intricate and random to be completely explained by deterministic tools.

5 Stochastic modeling of nanoparticle catalysis

Nanocatalysts are fundamentally different from the bulk catalysts due to their high surface to volume ratios, structural heterogeneity, and flexibility. Structural heterogeneity can arise from different atomic configurations, leading to a diverse ensemble of sites on a single nanocatalyst.[138,139] Due to thermal fluctuations, adsorbate binding, and reaction environments, nanocatalysts can also undergo dynamic surface restructuring. For example, Pt nanoparticles can restructure to expose different facets in hydrogen evolution reactions.[140,141] Surface restructuring indicates that the nanocatalyst is not static but a statistical ensemble of several metastable configurations. The relative populations of metastable states can change in response to the reaction environment. Fluctuations in surface structure can also correlate with reaction rates, implying that dynamic site rearrangements can influence catalytic efficiency. In addition, nanocatalysts can have cooperativity across spatially distant sites. Evidence of cooperativity has been observed in single-molecule experiments, where distant catalytic sites on a nanoparticle can communicate synergistically *via* charged hole migration.[60,142] Fig. 3 summarizes these phenomena in a nanocatalyst. The origins of these phenomena lie in the nanoscale nature of the catalyst; therefore, understanding and leveraging heterogeneity, dynamics, and cooperativity together offer a powerful paradigm for designing next-generation nanocatalysts. Using the discrete state stochastic modeling approach, these properties of the nanocatalyst have been studied.[96–98,143,144] Using the concepts of stationary state and first passage time distributions, important dynamic properties of nanoparticle catalysis were evaluated. We also discuss

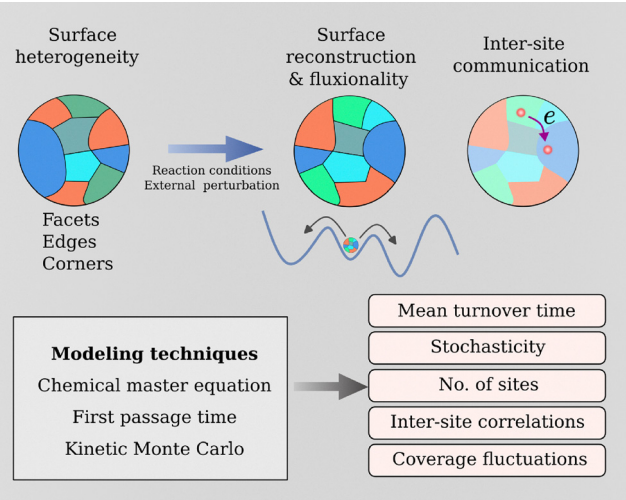

Fig. 3 Schematic diagram to unify the role of surface heterogeneity, fluxionality, and cooperativity. Surface sites can have multiple types due to spatial heterogeneity. Under reaction conditions or applied perturbation, the catalyst can access an ensemble of different structures with different activities. Charge transfer from one site to another can lead to cooperative communication between spatially distant sites. Stochastic modeling approaches can provide several practically important observables.

these studies and other similar works in this direction in the upcoming sections.

5.1 Modeling of a single reaction

The model of a single reaction involves the substrate S binding to a catalytic site, and *via* a sequence of reversible steps, the product is formed. To illustrate the utility of the CME, we take a toy example of a simple two-step reaction, similar to the Michaelis–Menten reaction, as shown in Fig. 2(a). Since we are interested in the rate of product formation, we can use the backward CME to solve this problem. Let $F(n,t)$ be the FPT probability density function of forming a product in time t initially starting from state n. Here $n \in \{S,\mathrm{CS}\}$ and C is the catalytic site, Au in Fig. 2(a). Using the backward CME the time evolution for $F(n,t)$ is written as

$$\frac{\mathrm{d}F(S,t)}{\mathrm{d}t} = k_1[\mathrm{S}]F(\mathrm{CS},t) - k_1[\mathrm{S}]F(S,t) \tag{11}$$

$$\frac{\mathrm{d}F(\mathrm{CS},t)}{\mathrm{d}t} = k_2\delta(t) + k_{-1}F(S,t) - (k_2+k_{-1})F(\mathrm{CS},t) \tag{12}$$

The mean rate of product formation obtained from the above equations is

$$\langle\tau\rangle^{-1} = \left(\int_0^\infty tF(S,t)\mathrm{d}t\right) = \frac{\frac{k_1}{k_{-1}}k_2[\mathrm{S}]}{1+\frac{k_1}{k_{-1}}[\mathrm{S}]+\frac{k_2}{k_{-1}}} \approx \frac{\frac{k_1}{k_{-1}}k_2[\mathrm{S}]}{1+\frac{k_1}{k_{-1}}[\mathrm{S}]}, \tag{13}$$

which is the same expression obtained from the ensemble methods (eqn (10)). This expression has been obtained by the renewal method described in ref. 144, which is quite similar to the first passage time approach. The explicit formula of the randomness parameter was calculated in this study, which was inaccessible in previous studies of similar catalytic systems.[14,16,71] The value of the randomness parameter obtained using eqn (7) can be written as

$$R = \frac{\left(\frac{k_2}{k_{-1}}\right)^2 + 2\frac{k_2}{k_{-1}} + \left(\frac{k_1}{k_{-1}}[\mathrm{S}]+1\right)^2}{\left(1+\frac{k_2}{k_{-1}}+\frac{k_1}{k_{-1}}[\mathrm{S}]\right)^2} \tag{14}$$

For the limiting case of the fast binding–unbinding rate, $k_2 \ll k_1,k_{-1}$, we obtain $R = 1$, indicating that product formation is the only rate limiting step in the reaction. Randomness parameter variation as a function of substrate is depicted in Fig. 4, where at a specific substrate concentration, the maximum stochasticity is observed, indicated by minima of R. Secondly, for the case of one catalytic site, the R approaches unity at extreme [S] values; however, this trend is changed at low [S], when two competing sites are present. This indicates that R can effectively distinguish a single reaction and two competing pathways. Though this study focused on the case of two active sites on the catalyst, the generalization of this was limited.[144]

Different classes of reactions can have different active sites on the nanocatalyst and show different catalytic activities. Several factors, such as geometric, electronic, and confinement effects, can heavily influence the activity of an active site and its length scales and timescales.[50] Analysis of single-catalytic-site systems is widely understood from the perspective of enzyme catalysis. However, nanoparticle catalysis has several

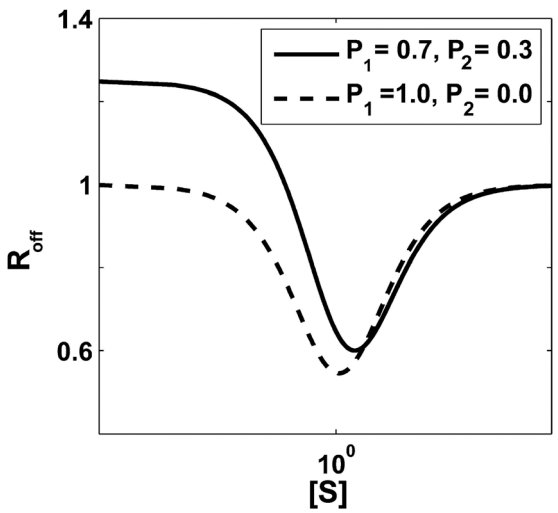

Fig. 4 Randomness parameter for a two site heterogeneous enzyme as a function of substrate S concentration. The dotted line is for the turnover from a single reaction and the solid line is for the turnover from two different reactions. P_1 and P_2 denote the fractional contribution of each reaction in the turnover. Reproduced from ref. 144, Copyright (2015), with permission from Elsevier.

complexities. First, the reaction mechanism from substrate adsorption to product formation can be complicated and can involve several intermediate states. Even the simplest reactions, such as hydrogen evolution and CO oxidation, can have a complex pathway.[147,148] Second, there are several active sites on a nanocatalyst.[50,149] Therefore, accounting for all the chemical processes in the theoretical analysis can be cumbersome.

Though single-molecule experiments have enabled us to measure single-turnover events on a single nanoparticle directly, they cannot describe the number of catalytically active sites on the nanoparticle, because a fluorescence burst due to the product can occur on any of the surface sites. Furthermore, these observations cannot explain how the statistics of catalytic turnover events and the turnover distributions are connected to the microscopic dynamics of catalytic reactions.

5.2 Effective kinetic scheme

A theoretical framework using a discrete state approach was proposed by Chaudhury *et al.* to efficiently account for the multiple sites on the catalyst.[150] Initially, this model was presented for a fixed number of active sites; however, in a further study, it was generalized for multiple reaction steps, a variable number of active sites, and heterogeneous active sites.[97,98] These studies present a general scheme to account for multiple reactions occurring in parallel on a nanocatalyst with N sites based on an effective kinetic scheme.

This scheme coarse-grains the multiple steps of the chemical reaction on an active site into effectually two states. First, when the catalytic site is empty and no substrate is attached to the site, and second, when the catalytic reaction is in the intermediate state, from where a single step can directly form a product. Essentially, there are only three effective transitions possible: (1) binding of the substrate to an empty site, which directly leads to the last intermediate state (the state just before product formation); (2) product formation (irreversibly) from the last intermediate state, which leads to an empty site and product; (3) dissociation of the last intermediate state all the way back to the substrate. Fig. 5(a) shows a schematic of a nanocatalyst with N active sites where a substrate S can bind and form the product. The reaction mechanism on a single active site is shown in Fig. 5(b) (upper), where a sequence of M steps leads to product formation.

Using the coarse-grained chemical process, the reaction on all catalytic sites can be easily projected onto the effective kinetic model.[98] Let n be the number of active sites present in the CS_M state on the catalyst; then, for an N site nanocatalyst system, the coarse-grained effective model has $N + 1$ possible effective states. The transition between the effective states is a 1D random walk like process, as shown in Fig. 5(b) (lower). A weighted average is carried out across all the effective states to obtain the turnover from a full catalyst, written as $\langle\tau\rangle$. The weighted average ensures that most probable effective state have larger contribution in the turnover time. Some of the limiting observations from these calculations are

$$\langle\tau\rangle \propto \frac{M}{N} \quad \text{and} \quad \lim_{N\to\infty} R = 1 \tag{15}$$

These studies showed that the mean reaction times in a catalytic system are inversely proportional to the number of active sites, irrespective of any chemical reaction taking place on the active site,[98,150] see Fig. 5(c). The turnover time increases linearly as a function of the intermediate steps in the reaction, depicted in Fig. 5(d). Also, stochastic fluctuations were quantified by the randomness parameter (R). As shown in Fig. 5(e), the randomness parameter is the smallest for one site ($N = 1$) and increases with increasing number of sites. For a larger catalyst size, the $R \approx 1$ indicates little stochastic fluctuations. Note that catalytic sites generally increase with a catalyst's size; however, this trend may not always be true. The randomness parameter result suggested that the stochastic effects in the dynamics are canceled out due to the averaging of noise by several chemical processes that take place independently at different catalytic sites.

Kang *et al.* have also proposed an experimental measure to estimate the number of active sites on the catalyst surface.[145] Using the counting statistics of turnover events of the catalyst, they investigated how the catalytic dynamics depend on the number of active sites and the reaction mechanisms. They also proposed that the turnover count statistic is a renewal process for longer time limits; therefore, their proposed measure becomes valid for a large time limit, even if an individual catalytic reaction may not be a renewal process. Their observation of randomness is shown in Fig. 5(f), where a minimum of randomness is observed with increasing reactant concentration (C_R/K_A). All these studies, utilizing various methodologies, complement each other in improving the understanding of catalytic dynamics.

5.3 Spatial heterogeneity in the nanocatalysts

The structural heterogeneity of nanocatalysts represented by the distribution in the size, morphology, and local coordination environment of the active sites is almost inevitable in practical nanocatalysts. Individual nanoparticles can differ in shape and size; however, a single nanoparticle can also have different surface sites. Many heterogeneous catalysts exhibit heterogeneity in the surface composition at the nanoscale level, resulting in multiple phases within the catalysts, which eventually can have distinct catalytic activities.[151,152] One of the first direct pieces of evidence for the different activities of various reactive sites coexisting on a supported metal catalyst was obtained using molecular-beam and *in situ* IR spectroscopy methods.[153,154] More recent single-molecule experimental studies have shown that different surface site types can be present even on a single nanoparticle. For example, active sites can be different at corners, edges and facets, and their catalytic features depend significantly on the morphology of the nanoparticle and the spatial location of active sites. Chen and coworkers have done a series of experimental works to understand the nanocatalysts at the microscopic level.[15,155–157] Using

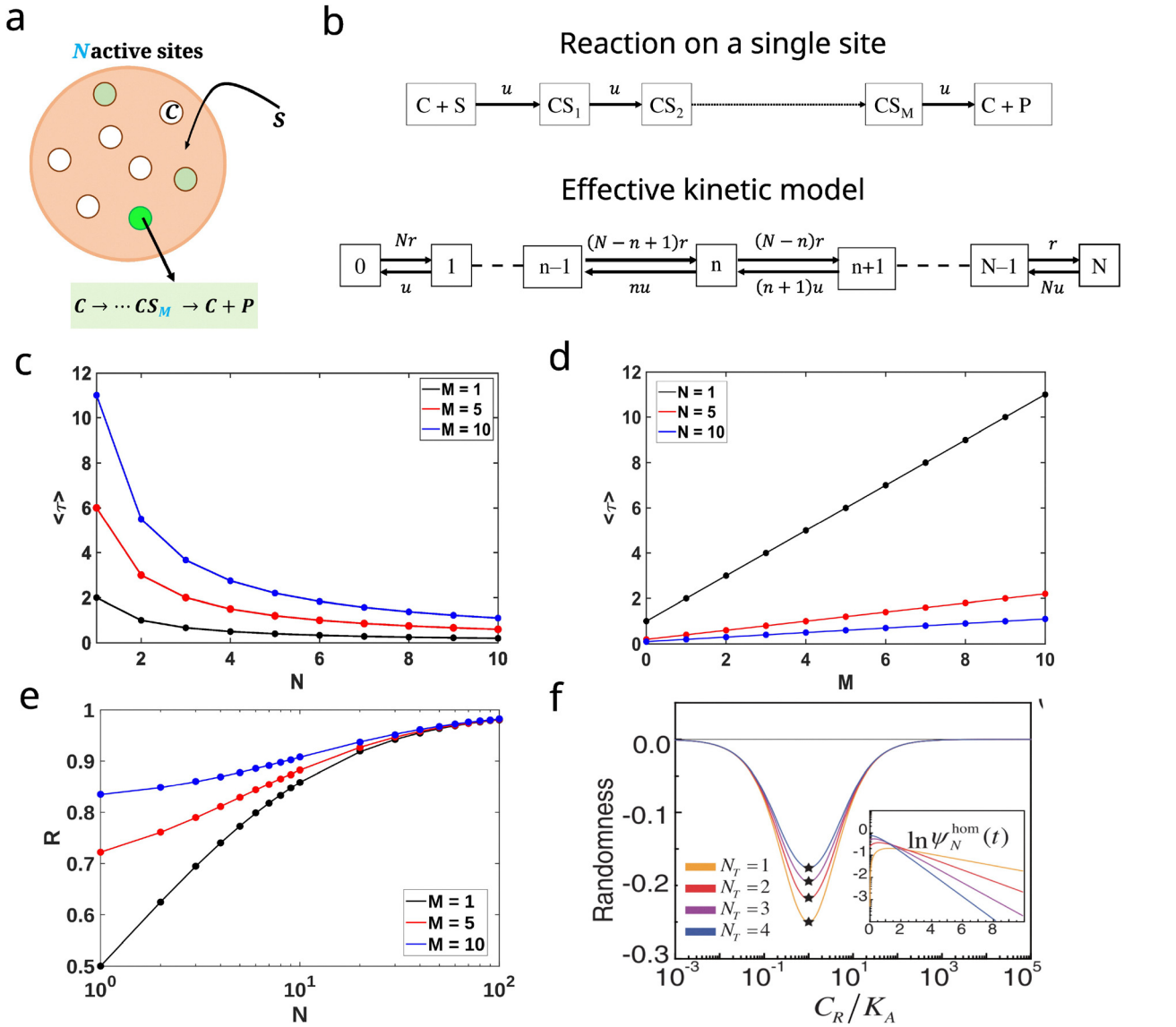

Fig. 5 Schematic representation of a nanoparticle catalyst with N identical catalytically active sites. (b) A simple representation of chemical reaction taking place on a single active site. (bottom) The effective kinetic model of the N site catalyst, where $r = u/M$ is the effective rate of reaching the CS_M state from C + S. The turnover rate as a function of (c) total catalytic sites on the nanoparticle and (d) the number of intermediate steps in the reaction pathway. (e) The randomness parameter varied with the number of catalytic sites. (f) The randomness parameter as a function of concentration of the substrate. (a)–(e) are reproduced with permission from ref. 98. Copyright 2021 American Chemical Society. (f) Reproduced with permission from ref. 145. Copyright 2021 American Physical Society.

super-resolution fluorescence microscopy, it has been observed that the same surface facets on the sides of a single nanorod exhibit reactivity that is not constant and exhibits a gradient from the center of the nanorod toward its two ends.[15] In another study, Chen and coworkers studied a 2D nanocrystal. In the nanocrystal, the activity of the catalyst is the lowest for the flat surface facets and the highest for the corner regions.[155] In anisotropically shaped photocatalyst particles, the different constituent facets may form interfacet junctions at their adjoining edges, and these interfacet junctions could lead to spatial variations of electronic and photoelectrochemical properties along the particle surface, even within the same facet, at near-edge regions showing different catalytic activities.[156,157] These findings have indicated that merely identifying the surface facets of nanocatalysts is not sufficient to correlate with and predict their reactivity, and a single nanoparticle can show significant heterogeneity in its activities.

In situ techniques have revealed that the exposed crystal facet also exerts a significant influence on both the quantity and nature of catalytically active sites, where within a single facet, the presence of various coordinatively unsaturated surface sites gives rise to distinct adsorption environments. For example, Zhang *et al.* showed that the intrinsic heterogeneity of conventionally synthesized supported Rh catalysts can offer distinct advantages in heterogeneous catalysis where isolated Rh species exhibit high activity for the initial dehydrogenation

step, whereas Rh ensemble sites display high efficiency in the subsequent transformation, a step for which isolated Rh sites are essentially inactive.[54] In such a case optimal catalytic performance is achieved only when both types of sites coexist, illustrating the beneficial role of heterogeneity in multistep catalytic processes. During the oxidation of 5-hydroxymethyl-2-furfural (HMF) on Pt nanocrystals, molecular O_2 tends to generate $^{\bullet}OH$ species on the Pt(100) facet and $^{\bullet}O_2^-$ species on the Pt(111) facet.[53] Relative to $^{\bullet}O_2^-$, the $^{\bullet}OH$ species formed on Pt(100) demonstrates a stronger ability to activate oxygen, thereby promoting aerobic oxidation of HMF through a dehydrogenation pathway.

Using stochastic methods, Chaudhury *et al.* presented a model to account for the underlying heterogeneity on the catalytic sites and heterogeneity on the reaction pathways,[97] as shown in Fig. 6(a). The mean turnover time from this model, for two different active sites, was found to be

$$\langle \tau \rangle_{N_1,N_2} = \frac{1+M}{N_1 a_1 + N_2 a_2} \tag{16}$$

Here, M is the number of intermediate steps in the reactions. A similar result was also observed in other studies.[145,150] It is argued that the application of the proposed theoretical approach to real nanocatalyst systems could uncover essential molecular details of the underlying chemical processes. There are three sources of heterogeneity in a catalytic system. First, we investigate the heterogeneity that arises as a result of the distribution of different types of sites. Second, heterogeneity in the chemical reaction (mechanism or the number of steps) occurs in the chemical reactions on the catalyst. Third, heterogeneity due to different activities of intermediate steps (though the number of steps may be the same). It was proposed that the

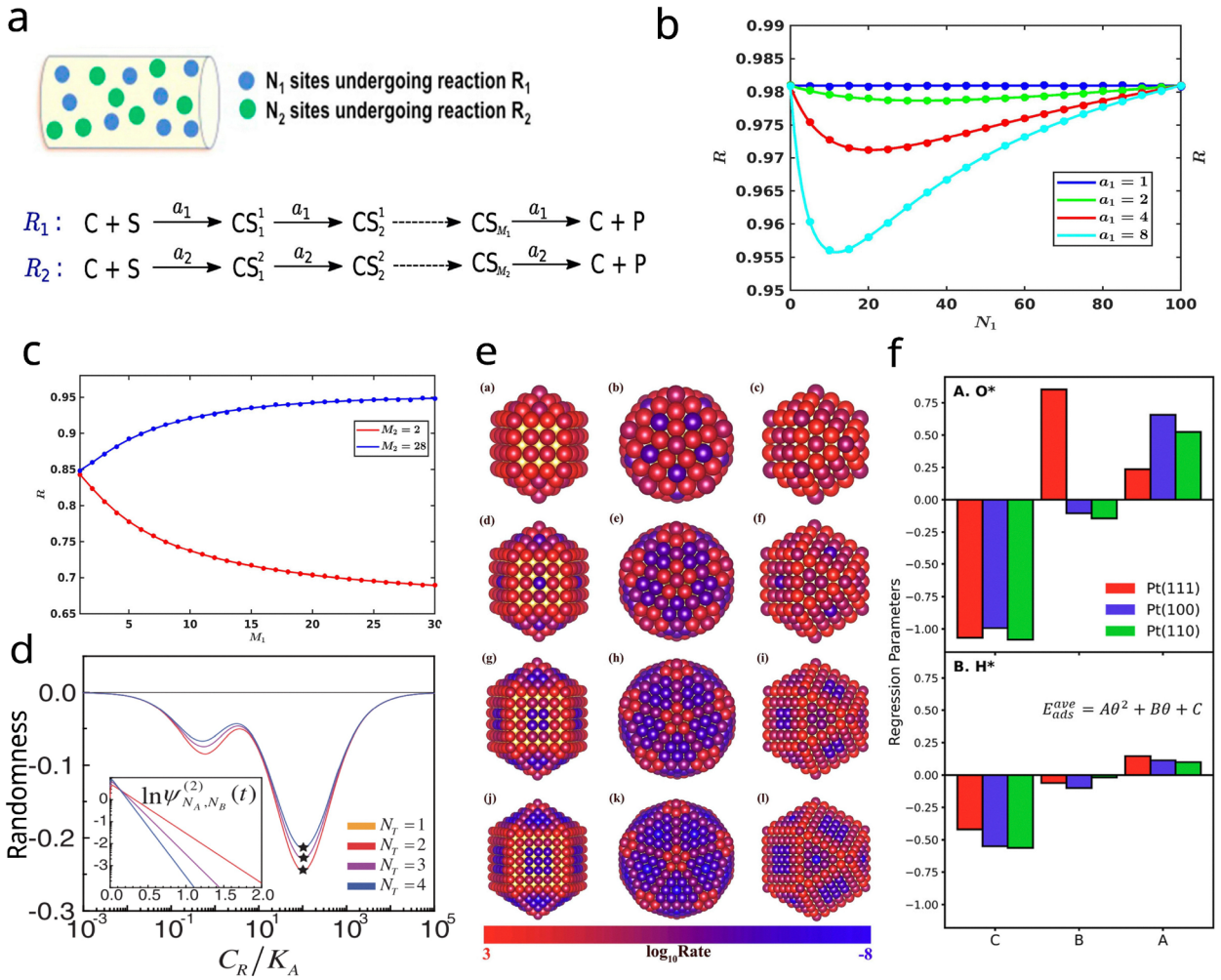

Fig. 6 Schematic representation of a nanoparticle catalyst with two different types of, N_1 and N_2, catalytically active sites. (bottom) The chemical reaction taking place on each type of site. The randomness parameter as a function of (b) N_1 while keeping N_2 constant and (c) M_1 while keeping M_2 constant. (d) Randomness for a heterogeneous model with substrate concentration. (e) CO oxidation rate schematic on surface sites of Au clusters of different geometries. (f) Fitted parameters A, B, and C for the adsorption energy model for O and H. (a)–(c) are reproduced from ref. 97, with permission from AIP Publishing. (d) is reproduced with permission from ref. 145. Copyright 2021 American Physical Society. (e) is reproduced with permission from ref. 146 Copyright 2018 American Chemical Society. (f) is reproduced with permission from ref. 34. Copyright 2024 American Chemical Society.

randomness parameter can capture these heterogeneities.[97] As shown in Fig. 6(b), when two competing pathways have similar contributions to turnover, the randomness parameter is the lowest, showing maximum stochastic fluctuation. In addition, heterogeneity in reaction pathways can have a dual effect based on the number of steps in the other active sites; see Fig. 6(c). A similar heterogeneous system studied by Kang *et al.*[145] showed that the randomness parameter shows a bistable behavior when the substrate concentration increases, as shown in Fig. 6(d).

Apart from these theoretical developments, several computational studies have been carried out to investigate heterogeneity. Wang *et al.* studied CO oxidation on an Au_x catalyst, where they obtained an optimized structure of the nanocatalyst using revised particle swarm optimization and DFT calculations.[33] They observed weak adsorption of CO and O_2 onto the face sites, which resulted in lower activity. Xu *et al.* investigated, using DFT calculations, how the geometric characteristics of nanoparticles determine the binding strength of surface adsorbates and, consequently, influence their catalytic activity,[146] as shown in Fig. 6(e). Omoniyi *et al.* developed a computational approach to analyze the effects of adsorbate–surface and adsorbate–adsorbate interactions on multifaceted platinum nanoparticles using DFT-based models.[34] This study finds strong repulsive lateral interactions for oxygen compared to hydrogen, see Fig. 6(f), which significantly impact adsorption behavior across different Pt facets and also depend on the adsorbate identity. Surface site heterogeneity studies have been carried out to investigate propane oxidative dehydrogenation on hydroxylated Ni-doped CeO_2 nanorods.[35]

6 Communicating catalytic sites

In an earlier discussion, the models presented had considered an important assumption that catalytic sites are independent. More specifically, the catalytic reaction on one active site does not influence the reaction on neighboring sites. This assumption is valid in most cases; however, it is far from reality, and communication between spatially separated catalytic sites exists in nature. Such communication has been well known for the catalytic allostery of enzymes, where binding or catalytic conversion of a substrate molecule at one site influences the binding or catalysis at another.[159,160] The fundamental reason behind the allostery is the communication *via* structural changes occurring at local and global scales, which are mediated by covalent bonds and intermolecular interactions.[161] The cooperativity is not limited to enzyme catalysts and has been confirmed experimentally in nanoparticles of various materials, where reactions at different surface sites on the same nanoparticle or single atom catalyst (SAC) can communicate.[60–63,162,163] In heterogeneous catalysis, the spillover effect enables product diffusion, connecting reactions at different sites on the same catalyst.[164,165] Investigation of the oxygen reduction reaction (ORR) on a single-atom $Fe–N_4$ catalyst has established the relationship between the inter-site distance and the turnover rate at individual sites.[62] Li *et al.* reported the presence of synergetic interactions between neighboring Pt monomers. These interactions cause distinct reaction pathways and can yield enhanced catalytic performance compared to isolated monomers in the CO_2 hydrogenation reaction.[63] A study conducted by Chen and co-workers reported intra-particle catalytic cooperativity during the catalysis of redox chemical reactions on Au and Pd nanoparticles.[60] Statistical analysis of Pearson's cross correlation coefficients (PCCs) between different segments of individual nanoparticles revealed that successive product-formation events were correlated with a temporal memory (or lifetime) of $\sim$10–100 s and a communication distance of $\sim$200–600 nm. Here the motion of positively charged holes is responsible for the observed catalytic communication and cooperativity.

Punia *et al.* presented a novel theoretical framework to investigate cooperative communication on the nanorod.[158] The model is based on the migration of charged holes created during a redox reaction to neighbouring segments on the nanorod. The theory assumes that the probability of the catalytic reaction to take place at a given active site depends on the local concentration of positively charged holes, and each redox reaction creates an additional amount of charged holes. By dividing the nanorod into segments of the same length, they proposed that the charged holes that are produced in any segment after a catalytic reaction (rate k) move to adjacent segments with a jump process (rate u) and disappear due to a finite lifetime (rate r), as shown in Fig. 7(a) (upper panel). This situation can be modeled as a birth-death-like process where a hole created at site zero has an equal probability to move in both directions, see Fig. 7(a) (lower panel). For a non-linear type nanoparticle, the hole migration can occur in two or three dimensions, which can be accounted for by using a similar approach. The stationary distribution of probabilities for finding the charged hole in a segment was calculated for the 1D model, and it was found that there is an increased probability to find the messenger (hole) at the same place where it was produced (n = 0), and the distribution exhibits exponential decay as the distance from the origin increases. This discrete state minimal model could also explain the existing correlation between two successive fluorescence burst events observed in the experimental research.[158] Fig. 7(b) shows the comparison of Pearson's correlation coefficient using this theoretical approach, and excellent quantitative agreement between theoretical predictions and experimental values was observed for all systems investigated, supporting the theoretical approach.[158] Thus, this theoretical framework could quantitatively describe the phenomena of catalytic communications from the microscopic point of view.

In a later study[143] the minimal model of homogeneous diffusion and death rates was extended to a heterogeneous case as the former did not account for inhomogeneity in the structural and dynamic properties of single nanocatalysts[25,31,155,166] where the diffusion rate and the decay rate of charged holes spatially vary along the nanoparticles (see Fig. 7(c)). Using this heterogeneous model, the communication lifetimes and correlation lengths were

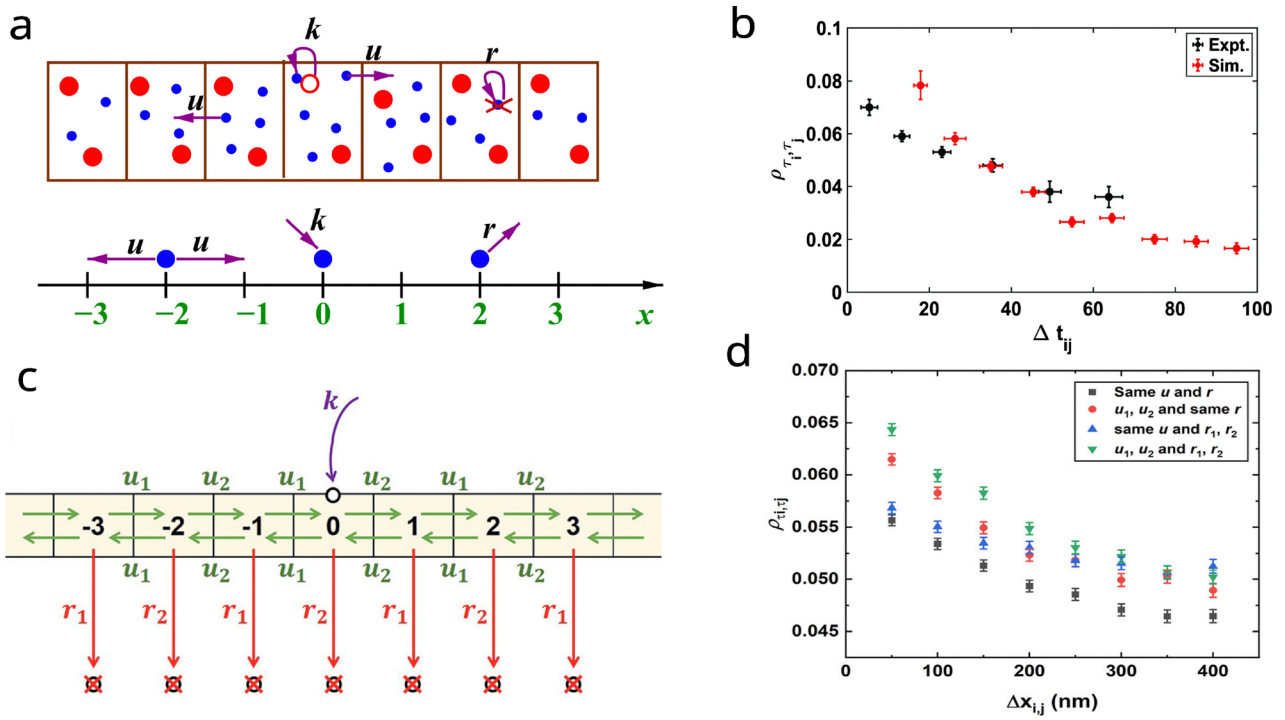

Fig. 7 Communication in the nanoparticle catalysis; (a) the schematic diagram of hole creation, migration, and disappearance on a nanorod is divided into segments of equal length. The panel at the bottom shows the discrete state model, where the lattice sites are labeled as integers for different segments. (b) Experimental and theoretical (simulated) Pearson's cross-correlation coefficients against average time separation Δt_{ij} of subsequent reactions at segments i and j on the Pd nanorod. (c) Model for catalytic communication with heterogeneous rate constants. (d) Pearson's cross-correlation coefficients varied with average separation Δx_{ij} for two segments i and j on the nanorod and comparison between heterogeneous and homogeneous cases. (a) and (b) are reproduced from ref. 158 published by PNAS under CC BY-NC-ND 4.0. (c) and (d) are reproduced with permission from ref. 143. Copyright 2023 American Chemical Society.

calculated, which revealed that spatial heterogeneity can increase the strength of cooperativity, while the communication lifetimes and distances decrease (see Fig. 7(d)).[143] In addition, the impact of surface restructuring on catalytic communication was also modeled as stochastic transitions between macrostates with different dynamic properties of charged holes.[167] This study revealed that communication times always decrease with increasing rates of dynamic restructuring, while communication lengths exhibit a dynamic behavior that depends on how dynamic fluctuations affect the migration and death rates of charged holes.[167] All of these findings provide information on microscopic understanding of cooperative communication and suggest potential strategies to improve catalytic efficiency.

7 Dynamic catalysis

In previous sections, we have discussed a class of catalysts in which the rate of reaction occurring on a nanoparticle site is constant throughout the reaction. This type of catalyst is termed the static catalyst. The turnover rate of a static catalyst has a fundamental limit based on the Sabatier principle.[172,173] The principle says that the highest turnover from a catalyst can be obtained under the condition of intermediate interactions between the substrate and the catalytic sites. The dissociation of the product from the catalyst becomes the rate-limiting step for strong interactions. For very weak interactions, substrate binding to the site becomes the rate-limiting step. In both extreme cases, the catalyst efficiency is the lowest and leads to a volcano-type relation between the turnover rate and the substrate-catalyst binding energy.[174,175] The Sabatier principle has been crucial in the conceptual understanding and design of new catalyst materials.

Recently, another type of catalytic system has been investigated in which reaction rates can change in real time, known as dynamic catalysts. This has led the researchers to examine whether the activity fluctuations can be utilized to enhance or control the catalysis. Fluctuations in the shape, surface and activities of the nanoparticles are already well known in the literature.[176–180] Simulation studies have suggested that surface modifications by an external perturbation can lead to a higher catalytic turnover rate. Modification of the surface can be achieved by external electric fields,[181–184] charge fluctuations, and mechanical forces.[185–188] The work of Dauenhauer and co-workers showed that if the energies of intermediate species in the chemical reaction are changed periodically, it can lead to high efficiency, which is beyond the Sabatier limit.[189–192] At a specific frequency of periodic switching, a resonance is established where the catalysts show a maximum turnover rate; therefore, these are called resonance catalysts.[193,194] Some initial experimental observations support the idea that catalytic

efficiency can be improved in dynamic catalysis.[195] The basic working principle of resonance catalysts can be explained by Fig. 8(a), which shows an energy diagram of A(g) → B(g) reaction *via* two intermediates A* and B*. By altering the energies of intermediates A* and B*, the activation barrier of the reaction steps can be modified, as indicated by the blue and green colors. It is noteworthy that the transition A* → B* is faster in the green state, and the transition B* → B(g) is faster in the blue energy diagram. The periodic fluctuations between the blue and green energy curves lead to a low-barrier pathway in the reaction by coupling of elementary steps with the oscillations of the catalyst. A Sabatier volcano plot for the static catalyst case is shown in orange color in Fig. 8(b), where a red dot indicates the optimum turnover frequency for a single reaction pathway. By changing the binding energy of B* periodically (at a certain frequency range) the turnover frequency from a dynamic system can surpass the Sabatier optimum, the purple line. Resonance catalysts demonstrate that the fluctuations can be utilized to overcome the Sabatier limit, challenging the traditional notion of a static catalyst in terms of catalytic dynamics and efficiency.

In addition to forced fluctuations, passive fluctuations also exist in the fluxional catalysts. Fluxional catalysts are a class of dynamic catalysts where the fluctuations in the activity or surface are not forced periodically; rather, they stochastically interconvert between several isomeric states due to thermal fluctuation. Each of these isomeric states can have different activities in the chemical reaction. Dynamic restructuring of catalytic sites has been reported in various bulk catalytic surfaces, nanoparticle systems, and supported nanocluster catalysts.[43–45] Some metal nanoclusters have shown dynamic meta-stability at the atomic scale, where they can transition to multiple low energy states, exhibiting different catalytic activities.[43–45] Nanocatalysts tend to undergo restructuring under external stimuli during catalytic reactions, which is triggered by nonequilibrium external parameters such as reaction temperature, atmosphere, surface adsorbates, electric field, pH, *etc.*[58,138] The dynamic transformation can range from the atomic scale to phase changes at the large scale, which has been observed in *in situ* operando experiments. For example, the surfaces of Pd and Pt nanoparticles show an oscillatory characteristic during CO oxidation.[42] Crozier and coworkers have experimentally demonstrated dynamic structural reconfigurations on CeO_2-supported catalysts Pt, which are correlated with the catalysis process.[40,41] Surface-specific restructuring behavior was also reported in high-entropy alloys.[37,196,197] Pulsed electrolysis is a promising method for directing reactions due to its ability to modulate the oxidation state of the catalyst by periodically applying an oxidative-reductive potential.[198–200] Using this method, the concentrations of H^+ and OH^- ions can be modified, thereby improving the selectivity and CO_2 reduction reaction.[199–202] Dynamic reconstructions open new pathways to strategically design catalysts with tailored behavior and facilitate the discovery of new phenomena in nanomaterials.

7.1 Dynamic catalysis minimal model

Several theoretical/simulation studies model the resonance catalysts by inducing periodic fluctuations in the energies of reaction species.[184,189,190] These studies have considered externally induced surface or temperature modifications. However, in the case of fluxional catalysts, the transitions between potential energy surfaces happen passively spontaneously and stochastically, which are governed by the intrinsic kinetics of chemical reactions.[203] A minimal model using a discrete-state stochastic approach was presented in a recent study by Jangid *et al.* to investigate dynamic catalysis.[96] The schematic picture of the model is shown in Fig. 8(d) along with the reaction mechanisms on the different surfaces. This is a minimal model where the catalytic surface can fluctuate between two surfaces A and B, where two different reactions can take place. At any instant of time, every active site can be found in one of the four microstates: free A site, free B site, A site occupied by the CS complex, and B site occupied by the CS* complex. Fig. 8(e) shows the effective model described in Section 5.2, for the dynamic catalyst with two active sites, which consist of all physical–chemical processes of the catalyst. This model was solved analytically for the steady-state probabilities using the CME to obtain relevant quantities for $N = 2$ active sites.[96] The idea was to use the simplest theoretical model to obtain a microscopic picture of underlying processes and answer some fundamental questions regarding such catalytic systems. For example, can the dynamic catalyst always provide a high turnover rate, and what is the microscopic reason? If so, what is the driving force behind the possible enhancements in catalytic performance in dynamic catalysis? Using this theoretical formalism, the mean reaction times for static catalysts (written as $\langle\tau\rangle_s$) and dynamic catalysts (written as $\langle\tau\rangle_d$) were calculated and a dimensionless parameter known as the efficiency function EF, which is the ratio of these reaction times, was evaluated.[96]

$$\mathrm{EF} = \frac{\langle\tau\rangle_s}{\langle\tau\rangle_d} \tag{17}$$

EF > 1 indicates that dynamic catalysis is more efficient than static catalysis. Similarly, EF < 1 denotes that the static catalyst is more efficient and EF = 1 indicates that the static and dynamic catalysts have the same efficiency. EF can be easily measured in experiments, as it is the ratio of turnover rates. We now demonstrate how the efficiency of dynamic catalysis can be improved. Consider a scenario in which the transition S → CS is faster compared to CS → P, for a type-A surface, see Fig. 8(f). Here, the product formation step is rate-limiting. If there is a dynamic fluctuation to additional surface, type-B, and the energy barriers of type-B are asymmetric (left panel of Fig. 8(f)), then S → CS → CS* → P becomes a minimum energy pathway, due to dynamic transition CS → CS*. Thus binding of the substrate on a type-A surface and formation of a product from a type-B surface lead to kinetic asymmetry that can be utilized to obtain a high turnover rate. Conversely, if the barriers of type-A and type-B surfaces are symmetric (the right panel of Fig. 8(f)), then product formation always remains a

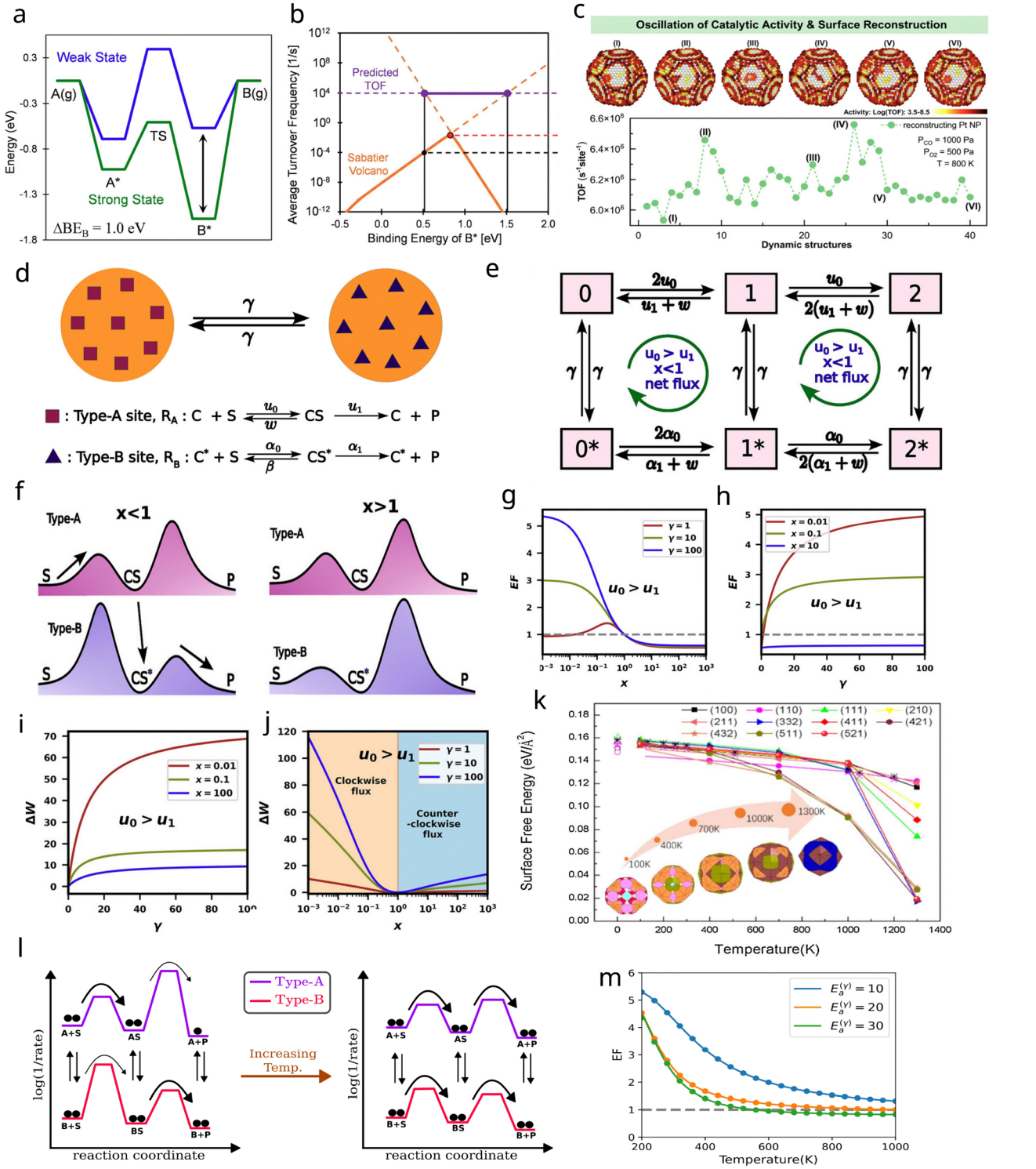

Fig. 8 Dynamic restructuring in catalysis. (a) Different energy pathways for reaction A(g) → B(g) *via* intermediates A* and B* (b) Sabatier volcano plot (orange) and dynamic catalyst turnover rate (purple) for different fluctuation energies. (c) Activity map of different surface reconstructions, along with their turnover frequencies. (d) Schematic representation of a nanocatalyst transitioning between two surface states with different active sites. The mechanisms of chemical reactions on the active sites are illustrated below. (e) An effective kinetic model for a catalyst with two sites. (f) Energy diagram for two cases for the dynamic catalyst. (g), (h) The efficiency of the dynamic catalyst compared to the static catalyst. (i), (j) The rate of energy dissipation in the dynamic catalysis. (k) Effect of temperature on surface energies of different faces of a nanocatalyst. (l) A schematic diagram illustrating the effect of temperature on the rates of the dynamic catalyst. (m) shows that the efficiency of the dynamic catalyst varies with temperature. (a) and (b) are reproduced with permission from ref. 168. Copyright 2025 American Chemical Society. (c) is adapted from ref. 169 licensed under CC-BY-NC-ND 4.0 Copyright (2024) The Authors, published by American Chemical Society. (d)–(j) are reproduced with permission from ref. 96. Copyright 2024 American Chemical Society. (k) is adapted from ref. 170, Copyright (2020), with permission from Elsevier. (l) and (m) are reproduced with permission from ref. 171. Copyright 2025 American Chemical Society.

rate-limiting step. In that case, dynamic transitions offer no advantage and even reduce the catalytic efficiency due to additional unproductive steps. Fig. 8(g) shows the efficiency function relative to the static catalyst, where it achieves greater than one value for a certain range of parameter values. In addition, the fluctuation rate increases the efficiency, as shown in Fig. 8(h). These results indicated that the enhancement in efficiency in dynamic catalysis is conditional, which is only true for some specific ranges of kinetic parameters.

7.2 Energy dissipation in dynamic catalysis

The high turnover rate of the dynamic catalyst is obtained when the system can escape or avoid large kinetic barriers. Such situations are only possible when cyclic fluxes in the reaction pathways lead to energy dissipation in the system. The concept of energy dissipation from stochastic thermodynamics has been useful in the study of small-scale systems such as colloidal particles[204] and molecular motors.[205,206] Application of external driving forces to these systems can lead to a non-equilibrium steady state. Investigating energy dissipation is relevant as it quantifies the cost of sustaining a system and provides a quantitative tool for distinguishing between systems with different degrees of deviations from equilibrium. For a discrete-state Markovian jump process, the energy dissipation is given by[206–208]

$$\Delta W = \frac{1}{2}\sum_{i,j}\left(r_{ij}P_j - r_{ji}P_i\right)\ln\left(\frac{r_{ij}P_j}{r_{ji}P_i}\right) \tag{18}$$

where P_i is the steady-state probability of state i and r_{ji} is the transition rate from state i to j. Using an effective kinetic model, the theoretical method assessed energy dissipation and its relation with the efficiency of dynamic catalysis. Due to a high fluctuation rate γ the cyclic fluxes in the catalytic system (Fig. 8(e)) increase, leading to high energy dissipation, see Fig. 8(i). Fig. 8(j) shows the energy dissipation as a function of the parameter x (given by $x = \alpha_0/u_0$), where the net energy dissipation occurs in the system for $x \neq 1$. Note that $x = 1$ denotes the case of a static catalyst where the energy dissipation is zero. In addition, this approach has predicted net cyclic flux, the direction of flux, and its role in the efficiency of dynamic catalysts.

Peters did a similar study on fluxional dynamic catalysts, where steady-state turnover frequencies, pathway fluxes, intermediate abundances, and transient intermediate relaxation rates were explicitly calculated.[132] It was also suggested that deviations from equilibrium might be an important aspect of these catalysts; the same conclusion was also reached in other studies.[96,184]

7.3 Effect of temperature on the dynamic catalysis efficiency

Temperature is one of the most commonly controlled parameters in the reactions. So, the natural question that arises is how does temperature play a role in dynamic catalysis? The metastable isomers of the nanoclusters show significant catalytic activities that are accessible in catalysis due to thermal fluctuations.[43–45,209] Temperature has been shown to play a key role in determining the relative fractions of the metastable isomers and reaction species, the activation energies, and the equilibrium constants.[210,211] Xing *et al.* investigated the dependence of temperature on the iron and iron carbide nanoparticle morphology.[170] They showed that bulk and surface free energies decrease parabolically with increasing temperature, due to entropic effects, see Fig. 8(k). At low temperatures, nanoparticles are dominated by low Miller index facets, and above a critical temperature, high Miller index surfaces begin to dominate. Therefore, temperature and entropy govern morphology evolution in nanocatalysts and can be utilized for tailoring structures to enhance catalytic performance.

Jangid *et al.* extended the minimal model of the dynamic catalyst to account for the temperature and partial fluctuations occurring at the active sites.[171] This study showed that increasing the temperature can disrupt the kinetic balance established to maintain high efficiency, where at high temperature all transitions become faster, see Fig. 8(l), and with increasing temperature, the efficiency can decrease; see Fig. 8(m). This is a significant result, as an increase in temperature leads to a faster turnover rate; however, the increment can be slow relative to the static catalyst.[171]

8 Theoretical modeling for understanding and designing catalysts

By modeling Markov jump processes, discrete state stochastic methods play an important role in understanding and designing novel catalysts. These methods explicitly represent the probabilistic jumps between well defined states, such as reactants, intermediates and products at single site resolution, therefore capturing spatial heterogeneity, fluctuations and rare events. These models can link energies obtained from *ab initio* DFT calculations for accurate prediction of catalytic activity and selectivity under operating conditions. The distribution and lifetime of discrete states can be utilized to identify which site types and structural motifs dominate the reactivity. Knowledge about individual discrete states can be used to suppress undesirable states and can help optimize catalyst architecture, such as size, shape, facet exposure, or even composition, to stabilize most productive reaction states.

As we have discussed previously, discrete state stochastic models can provide a rigorous framework to characterize catalysis *via* approaches such as CME, FPT, KMC, and stochastic fluctuations quantified by higher time moments and guide catalyst design by providing quantitative and qualitative insights at single site resolution. For example, the use of the randomness parameter can uncover the possibility of hidden intermediate states, multiple parallel pathways, the possibility of inhibition and distinguish fast and selective pathways from slow and nonselective pathways, therefore indicating which site type, surface motifs, or mechanistic pathways are responsible for observed reactivity,[93,94,97,98,145] consequently enabling desired modifications such as facet engineering, alloying, and

ligand selectivity for high performance catalysts.[212–214] These models go beyond the assumption that all sites are equal, showing that different local configurations of adsorbate molecules can have different kinetics.[215] The concept of microscopic cooperative communication among catalytic sites allows one to predict and design catalysts that can maximize this synergistic effect, leading to enhanced reaction rates, higher selectivity, and improved catalytic efficiency.[60,143,158] By discretizing hole dynamics into a discrete space, the spatial movement of charge carriers can be easily quantified, helping in understanding the spatial correlation length and temporal memory. Dynamic catalysis has the potential to fundamentally shift the optimum catalytic limit imposed by the Sabatier principle, where, by actively modulating the binding energies or rates, one can transiently decouple elementary reaction steps (adsorption, reaction, and desorption) and surpass the classical volcano plot maximum.[96,172,193] In this way, stochastic modeling can transform single-particle catalytic fluctuations into actionable design principles, mapping the structure and mechanism to performance.

9 Summary and outlook

Heterogeneous catalysts are highly complex and uncovering the underlying microscopic mechanisms is crucial to advancing catalytic science. This article provides a concise overview of theoretical development in single-nanocatalyst characterization, including recent experimental advances and computational methods. Single-molecule fluorescence spectroscopy and operando characterization techniques have provided remarkable insights into these tiny structures in experimental studies, enabling the detection of heterogeneity, cooperativity, and the dynamic evolution of catalysts in real time under reaction conditions.[71,155,216] We discussed a general and robust framework of effective kinetic modeling based on discrete state stochastic methods that can be used to account for all chemical reactions on the nanocatalyst.[150] The advantage of the stochastic approach is that one can analytically evaluate physical–chemical processes and the dynamic properties of single nanocatalysts by accounting for stochastic fluctuations.[95] We have recalled recent theoretical studies that have uncovered the molecular mechanisms of nanoparticle catalysis. We noted that the underlying heterogeneity in the catalysis can be used as a valuable quantitative tool to understand the microscopic mechanisms of catalytic systems and can be used to quantify the number of active sites.[97,98] The theoretical model of dynamic catalysis can help researchers identify the bottlenecks for designing catalytic materials that may break the traditional Sabatier limit and outperform traditional catalysts.[96] The theories of cooperative communications between different segments on the nanorod provide an effective quasiclassical qualitative description of catalytic communication, which might help to improve catalytic efficiency.[143,158,167]

The disadvantage of stochastic approaches is that they are difficult to solve analytically for a large and complex catalytic system. As a result, some simplifications and assumptions are made in the analysis, which may restrict the full quantitative description. For example, in the heterogeneity model, Fig. 6, the backward chemical transitions were ignored, the rates for a mechanism were assumed to be the same, and only two types of sites were considered.[97] The model could provide valuable qualitative insights, but the quantitative application to real systems can be limited. The communication model in Fig. 7 assumes that the holes reach a steady state quickly after creation. However, this assumption may not hold for all systems and requires further examination. The dynamic catalysis model presented here, Fig. 8, used a simple chemical reaction, but the impact of dynamic fluctuations remains poorly understood for more complex catalytic mechanisms.[96] These limitations and simplifications pave the way for further investigation of these systems and resolution of the limitations. One could examine the role of two or more substrates in the reaction[217,218] and the effect of external conditions such as temperature,[219] pH,[220] and the possibility of inhibition[221] in heterogeneous and dynamic catalysis models. In the communication model,[158] only one hole (charge carrier) was considered in the communication mechanism; however, it would be interesting to consider the interactions of multiple charge carriers working together.[222] The model for catalytic cooperativity holds good only for intraparticle communication within the same nanorod. Furthermore, experiments have also reported communication between individual nanocatalysts with communication distances on the order of micrometers.[60] It has been established that such communications occur *via* molecular diffusion and are limited to selected systems.

While the state-of-the-art techniques in theoretical and computational catalysis have provided valuable mechanistic understanding in catalysis, the challenge lies in bridging the gap between idealized models and real catalytic complexity: from *ab initio* calculations to detailed kinetic modeling. Though developing simplified models can account for surface reconstructions and spatiotemporal heterogeneities, these factors are still difficult to fully capture within current mesoscale models. These models assume a well stirred reaction mixture while ignoring intermediate spatiotemporal effects such as transport and partial access of reactants to the active site. These effects have been incorporated in some studies; however, it still remains a challenge on a broader scale.[118,139,223] Accounting for these factors in the models is computationally challenging. Solvent effects introduce additional complexity due to fluctuating local environments, long range electrostatic interactions and entropic effects.[224–227] Simplified models of continuum or implicit solvation fail to capture solvent effects that are crucial for predicting true catalytic behavior.[226] Accurate modeling of such systems will require a combination of *ab initio* methods and sampling techniques with microkinetic and stochastic modeling, which is a computationally demanding task.

Machine learning has evolved from a niche research area to a powerful tool in the field of catalysis. ML is effective at extracting information from experimental or simulation data

without detailed knowledge of physical or chemical processes. The neural network potentials trained on DFT data can accurately reproduce *ab initio* energies and enable simulation of large systems.[228–230] These approaches facilitate the fast screening of catalyst materials and the estimation of kinetic parameters and establish relationships between the structures of catalysts and their physicochemical properties, catalytic performance and selectivity. By encoding physical constraints directly into neural network architectures, these models can achieve improved accuracy. For example, physics-constrained loss functions that incorporate mass and energy conservation laws can ensure that predictions remain physically consistent.[231,232]

In conclusion, suitable modeling approaches can significantly improve our understanding of the experimentally observed data and even help us make predictions. The results obtained from single-molecule studies, advanced spectroscopic techniques, and atomistic simulations in stochastic frameworks can complement and further refine our understanding of catalytic dynamics.[4,233] The accuracy of theoretical models for catalytic reactions can be greatly improved by developing state-of-the-art machine learning models.[234,235] Physically relevant models can help catalyst design and enable the development of more sustainable and efficient catalytic materials to meet industrial and environmental needs.

Conflicts of interest

There are no conflicts to declare.

Data availability

No primary research results, software or code have been included, and no new data were generated or analyzed as part of this review.

Acknowledgements

PJ acknowledges IISER Pune for the fellowship. SC acknowledges support from the SERB Power Fellowship (SPF/2022/000155).

Notes and references

1 J. K. Nørskov, F. Studt, F. Abild-Pedersen and T. Bligaard, *Fundamental Concepts in Heterogeneous Catalysis*, Wiley, 2014.
2 C. M. Friend and B. Xu, *Acc. Chem. Res.*, 2017, **50**, 517521.
3 J. K. Nørskov, T. Bligaard, J. Rossmeisl and C. H. Christensen, *Nat. Chem.*, 2009, **1**, 37–46.
4 A. H. Motagamwala and J. A. Dumesic, *Chem. Rev.*, 2020, **121**, 1049–1076.
5 T. Ishida, T. Murayama, A. Taketoshi and M. Haruta, *Chem. Rev.*, 2019, **120**, 464–525.
6 D. Astruc, *Chem. Rev.*, 2020, **120**, 461–463.
7 S. Guo, S. Zhang and S. Sun, *Angew. Chem., Int. Ed.*, 2013, **52**, 8526–8544.
8 K. An and G. A. Somorjai, *ChemCatChem*, 2012, **4**, 1512–1524.
9 I. Lee, F. Delbecq, R. Morales, M. A. Albiter and F. Zaera, *Nat. Mater.*, 2009, **8**, 132–138.
10 S. Zhang, X. Zhang, G. Jiang, H. Zhu, S. Guo, D. Su, G. Lu and S. Sun, *J. Am. Chem. Soc.*, 2014, **136**, 7734–7739.
11 W. Fu, H. Cao and A. K. Cheetham, *Adv. Opt. Mater.*, 2023, **11**, 2300434.
12 L. Huang, Q. Liu, W. Wu, G. Gao, X. Zheng, J. Wang and S. Dong, *Nat. Commun.*, 2023, **14**, 5594.
13 W. Xu, J. S. Kong and P. Chen, *J. Phys. Chem. C*, 2009, **113**, 2393–2404.
14 X. Zhou, W. Xu, G. Liu, D. Panda and P. Chen, *J. Am. Chem. Soc.*, 2009, **132**, 138–146.
15 X. Zhou, N. M. Andoy, G. Liu, E. Choudhary, K.-S. Han, H. Shen and P. Chen, *Nat. Nanotechnol.*, 2012, **7**, 237–241.
16 W. Xu, H. Shen, Y. J. Kim, X. Zhou, G. Liu, J. Park and P. Chen, *Nano Lett.*, 2009, **9**, 3968–3973.
17 F. Huang, D. Zhang, X. Mei, B. Zhang, J. Bao, P. Song, C. Han and W. Xu, *Carbon Neutralization*, 2025, **4**, e70002.
18 Y. Yang, Y. Ma and J. J. Gooding, *Faraday Discuss.*, 2025, **257**, 333–343.
19 J. S. I. Bryan, S. A. Tashev, M. Fazel, M. Scheckenbach, P. Tinnefeld, D.-P. Herten and S. Pressé, *J. Phys. Chem. B*, 2025, **129**, 4670–4681.
20 X. Liu, X. Ge, J. Cao, Y. Xiao, Y. Wang, W. Zhang, P. Song and W. Xu, *Proc. Natl. Acad. Sci. U. S. A.*, 2022, **119**, e2114639119.
21 A. Sathyan, E. Archontakis, A. J. H. Spiering, L. Albertazzi and A. R. A. Palmans, *Molecules*, 2024, **29**, 1850.
22 D. I. Njoku, Q. Guo, W. Dai, J. L. Chen, G. Mao, Q. Sun, H. Sun and Y.-K. Peng, *TrAC, Trends Anal. Chem.*, 2023, **167**, 117288.
23 J. B. Sambur and P. Chen, *Annu. Rev. Phys. Chem.*, 2014, **65**, 395–422.
24 C. Yan, J. Bao, P. Song and W. Xu, *J. Phys. Chem. C*, 2024, **128**, 13937–13943.
25 W. Xu, J. S. Kong and P. Chen, *Phys. Chem. Chem. Phys.*, 2009, **11**, 2767.
26 X. Mao and P. Chen, *Nat. Mater.*, 2022, **21**, 331–337.
27 H. Shen, W. Xu and P. Chen, *Phys. Chem. Chem. Phys.*, 2010, **12**, 6555.
28 T. Chen, Y. Zhang and W. Xu, *Phys. Chem. Chem. Phys.*, 2016, **18**, 22494–22502.
29 D. Devasia and P. K. Jain, *J. Phys. Chem. C*, 2021, **125**, 17734–17741.
30 T. Chen, S. Chen, Y. Zhang, Y. Qi, Y. Zhao, W. Xu and J. Zeng, *Angew. Chem., Int. Ed.*, 2016, **128**, 1871–1875.
31 T. Chen, S. Chen, P. Song, Y. Zhang, H. Su, W. Xu and J. Zeng, *ACS Catal.*, 2017, **7**, 2967–2972.
32 B. Zhang, D. Zhang, J. Bao, C. Han, P. Song and W. Xu, *Analyst*, 2024, **149**, 5184–5190.
33 Y. Wang, H. Xu, J. Zhu and D. Cheng, *Nanoscale*, 2024, **16**, 18871–18881.

34 A. Omoniyi and A. J. R. Hensley, *J. Phys. Chem. C*, 2024, **128**, 7073–7086.
35 A. P. Pushkar and J. J. Varghese, *J. Catal.*, 2022, **413**, 681–691.
36 C. A. Casey-Stevens, S. G. Lambie, C. Ruffman, E. SkÃ°lason and A. L. Garden, *J. Phys. Chem. C*, 2019, **123**, 30458–30466.
37 A. L. Maulana, P.-C. Chen, Z. Shi, Y. Yang, C. Lizandara-Pueyo, F. Seeler, H. D. Abruña, D. Muller, K. Schierle-Arndt and P. Yang, *Nano Lett.*, 2023, **23**, 6637–6644.
38 Y. Yang, H. Zhang and J. F. Douglas, *ACS Nano*, 2014, **8**, 7465–7477.
39 Y.-C. Lin, W. K. Kim and J. Dzubiella, *J. Phys. Chem. C*, 2020, **124**, 24204–24214.
40 J. L. Vincent and P. A. Crozier, *Nat. Commun.*, 2021, **12**, 5789.
41 E. L. Lawrence, B. D. A. Levin, T. Boland, S. L. Y. Chang and P. A. Crozier, *ACS Nano*, 2021, **15**, 2624–2634.
42 T. Ghosh, J. M. Arce-Ramos, W.-Q. Li, H. Yan, S. W. Chee, A. Genest and U. Mirsaidov, *Nat. Commun.*, 2022, **13**, 6176.
43 G. Sun, A. N. Alexandrova and P. Sautet, *J. Chem. Phys.*, 2019, **151**, 194703.
44 H. Zhai and A. N. Alexandrova, *J. Chem. Theory Comput.*, 2016, **12**, 6213–6226.
45 Z. Zhang, Z.-H. Cui, E. Jimenez-Izal, P. Sautet and A. N. Alexandrova, *ACS Catal.*, 2020, **10**, 13867–13877.
46 X. Duan, Y. Han, B. Zhu and Y. Gao, *Mater. Today Catal.*, 2023, **3**, 100032.
47 P.-C. Chen, C. Chen, Y. Yang, A. L. Maulana, J. Jin, J. Feijoo and P. Yang, *J. Am. Chem. Soc.*, 2023, **145**, 10116–10125.
48 J. Dong, Y. Xu, Z. Zhang and J. Feng, *Angew. Chem., Int. Ed.*, 2022, **61**, e202200187.
49 Y. Yang, S. Louisia, S. Yu, J. Jin, I. Roh, C. Chen, M. V. Fonseca Guzman, J. Feijóo, P.-C. Chen, H. Wang, C. J. Pollock, X. Huang, Y.-T. Shao, C. Wang, D. A. Muller, H. D. Abruña and P. Yang, *Nature*, 2023, **614**, 262–269.
50 C. Vogt and B. M. Weckhuysen, *Nat. Rev. Chem.*, 2022, **6**, 89–111.
51 Y. Xiao, Z. Guo, J. Cao, P. Song, B. Yang and W. Xu, *Proc. Natl. Acad. Sci. U. S. A.*, 2024, **121**, e2317205121.
52 M. Zhao, W. Li, M. Yang, Z. Zhao, R. Ye, X. Mao, P. Padgett and P. Chen, *Nat. Catal.*, 2024, **7**, 912–920.
53 Y. Liu, H.-Y. Ma, D. Lei, L.-L. Lou, S. Liu, W. Zhou, G.-C. Wang and K. Yu, *ACS Catal.*, 2019, **9**, 8306–8315.
54 J. Zhang, M. Wang, Z. Gao, X. Qin, Y. Xu, Z. Wang, W. Zhou and D. Ma, *J. Am. Chem. Soc.*, 2022, **144**, 5108–5115.
55 F. T. Haase, A. Rabe, F.-P. Schmidt, A. Herzog, H. S. Jeon, W. Frandsen, P. V. Narangoda, I. Spanos, K. Friedel Ortega, J. Timoshenko, T. Lunkenbein, M. Behrens, A. Bergmann, R. Schlögl and B. Roldan Cuenya, *J. Am. Chem. Soc.*, 2022, **144**, 12007–12019.
56 J. M. Rahm and P. Erhart, *J. Phys. Chem. C*, 2018, **122**, 28439–28445.
57 H.-W. Cheng, S. Wang, G. Chen, Z. Liu, D. Caracciolo, M. Madiou, S. Shan, J. Zhang, H. He, R. Che and C.-J. Zhong, *Adv. Energy Mater.*, 2022, **12**, 2202097.
58 H. Zhang, L. Chen, F. Dong, Z. Lu, E. Lv, X. Dong, H. Li, Z. Yuan, X. Peng, S. Yang, J. Qiu, Z. Guo and Z. Wen, *Energy Environ. Sci.*, 2024, **17**, 6435–6481.
59 Y. Nian, X. Huang, M. Liu, J. Zhang and Y. Han, *ACS Catal.*, 2023, **13**, 11164–11171.
60 N. Zou, X. Zhou, G. Chen, N. M. Andoy, W. Jung, G. Liu and P. Chen, *Nat. Chem.*, 2018, **10**, 607–614.
61 D. Xu, Y. Jin, B. He, X. Fang, G. Chen, W. Qu, C. Xu, J. Chen, Z. Ma, L. Chen, X. Tang, X. Liu, G. Wei and Y. Chen, *Nat. Commun.*, 2024, **15**, 8614.
62 Z. Jin, P. Li, Y. Meng, Z. Fang, D. Xiao and G. Yu, *Nat. Catal.*, 2021, **4**, 615–622.
63 H. Li, L. Wang, Y. Dai, Z. Pu, Z. Lao, Y. Chen, M. Wang, X. Zheng, J. Zhu, W. Zhang, R. Si, C. Ma and J. Zeng, *Nat. Nanotechnol.*, 2018, **13**, 411–417.
64 H. Kitano, *Nature*, 2002, **420**, 206–210.
65 L. Edelstein-Keshet, *Mathematical models in biology*, SIAM, 2005.
66 M. Besora and F. Maseras, *Wiley Interdiscip. Rev.: Comput. Mol. Sci.*, 2018, **8**, e1372.
67 J. A. Dumesic, *The Microkinetics of heterogeneous catalysis*, American Chemical Society, 1993.
68 T. Bligaard, J. Nørskov, S. Dahl, J. Matthiesen, C. Christensen and J. Sehested, *J. Catal.*, 2004, **224**, 206–217.
69 S. Matera, W. F. Schneider, A. Heyden and A. Savara, *ACS Catal.*, 2019, **9**, 6624–6647.
70 H. Lynggaard, A. Andreasen, C. Stegelmann and P. Stoltze, *Prog. Surf. Sci.*, 2004, **77**, 71–137.
71 W. Xu, J. S. Kong, Y.-T. E. Yeh and P. Chen, *Nat. Mater.*, 2008, **7**, 992–996.
72 M. Panigrahy, A. Kumar, S. Chowdhury and A. Dua, *J. Chem. Phys.*, 2019, **150**, 204119.
73 J. Goutsias, *Biophys. J.*, 2007, **92**, 2350–2365.
74 H. Ge and H. Qian, *J. R. Soc., Interface*, 2011, **8**, 107–116.
75 M. Jørgensen and H. Grönbeck, *ACS Catal.*, 2019, **9**, 8872–8881.
76 B. W. J. Chen, L. Xu and M. Mavrikakis, *Chem. Rev.*, 2020, **121**, 1007–1048.
77 C. W. Gardiner, *Handbook of stochastic methods for physics, chemistry and the natural sciences*, Springer-Verlag, 3rd edn, 2004, vol. 13, pp. xviii + 415.
78 H. Qian and L. M. Bishop, *Int. J. Mol. Sci.*, 2010, **11**, 3472–3500.
79 D. T. Gillespie, *J. Comput. Phys.*, 1976, **22**, 403–434.
80 D. T. Gillespie, *J. Phys. Chem.*, 1977, **81**, 2340–2361.
81 M. Stamatakis, *J. Phys.: Condens. Matter*, 2014, **27**, 013001.
82 M. Stamatakis and D. G. Vlachos, *ACS Catal.*, 2012, **2**, 2648–2663.
83 N. Van Kampen, *The Master Equation*, Elsevier, 2007, pp. 96–133.
84 G. Haag, *Modelling with the Master Equation*, Springer International Publishing, 2017.
85 J. Klafter and I. M. Sokolov, *First Steps in Random Walks: From Tools to Applications*, Oxford University Press, 2011.
86 S. Redner, *A Guide to First-Passage Processes*, Cambridge University Press, 2001.

87 D. J. Wilkinson, *Nat. Rev. Genet.*, 2009, **10**, 122–133.
88 V. Shahrezaei and P. S. Swain, *Curr. Opin. Biotechnol*, 2008, **19**, 369–374.
89 M. Henkel, H. Hinrichsen and S. Lübeck, *Non-Equilibrium Phase Transitions: Volume I: Absorbing Phase Transitions*, Springer, 2008.
90 K. Rajdl, P. Lansky and L. Kostal, *Front. Comput. Neurosci.*, 2020, **14**, 569049.
91 S. Chaudhury, J. Cao and N. A. Sinitsyn, *J. Phys. Chem. B*, 2013, **117**, 503–509.
92 S. Chaudhury, *J. Phys. Chem. B*, 2014, **118**, 10405–10412.
93 A. B. Kolomeisky, *Motor Proteins and Molecular Motors*, CRC Press, 2015.
94 S. C. Kou, B. J. Cherayil, W. Min, B. P. English and X. S. Xie, *J. Phys. Chem. B*, 2005, **109**, 19068–19081.
95 D. Singh, B. Punia and S. Chaudhury, *ACS Omega*, 2022, **7**, 47587–47600.
96 P. Jangid, S. Chaudhury and A. Kolomeisky, *J. Phys. Chem. C*, 2024, **128**, 9077–9089.
97 S. Chaudhury, P. Jangid and A. B. Kolomeisky, *J. Chem. Phys.*, 2023, **158**, 074101.
98 B. Punia, S. Chaudhury and A. B. Kolomeisky, *J. Phys. Chem. Lett.*, 2021, **12**, 11802–11810.
99 C. L. Vestergaard and M. Génois, *PLoS Comput. Biol.*, 2019, **15**, e1007190.
100 M. Boguná, L. F. Lafuerza, R. Toral and M. Á. Serrano, *Phys. Rev. E: Stat., Nonlinear, Soft Matter Phys.*, 2014, **90**, 042108.
101 N. Masuda and L. E. C. Rocha, *SIAM Rev.*, 2018, **60**, 95–115.
102 D. Y. Murzin, J. Wärnå, H. Haario and T. Salmi, *React. Kinet., Mech. Catal.*, 2021, **133**, 1–15.
103 G. Froment, *Chem. Eng. Sci.*, 1987, **42**, 1073–1087.
104 D. Y. Murzin and T. Salmi, *Catalytic kinetics*, Elsevier, 2005.
105 K. Reuter and M. Scheffler, *Phys. Rev. B: Condens. Matter Mater. Phys.*, 2006, **73**, 045433.
106 R. Van de Vijver, K. M. Van Geem and G. B. Marin, *Proc. Combust. Inst.*, 2019, **37**, 283–290.
107 Y. V. Suleimanov and W. H. Green, *J. Chem. Theory Comput.*, 2015, **11**, 4248–4259.
108 M. G. Evans and M. Polanyi, *Trans. Faraday Soc.*, 1936, **32**, 1333.
109 S. Garashchuk and D. J. Tannor, *Phys. Chem. Chem. Phys.*, 1999, **1**, 1081–1090.
110 J. K. Nørskov, F. Abild-Pedersen, F. Studt and T. Bligaard, *Proc. Natl. Acad. Sci. U. S. A.*, 2011, **108**, 937–943.
111 Z. Wang and P. Hu, *Phys. Chem. Chem. Phys.*, 2017, **19**, 5063–5069.
112 K. Honkala, A. Hellman, I. N. Remediakis, A. Logadottir, A. Carlsson, S. Dahl, C. H. Christensen and J. K. Nørskov, *Science*, 2005, **307**, 555–558.
113 D. T. Gillespie, *Annu. Rev. Phys. Chem.*, 2007, **58**, 35–55.
114 A. Jansen, *An Introduction to Kinetic Monte Carlo Simulations of Surface Reactions*, Springer, Berlin Heidelberg, 2012.
115 M. Jørgensen and H. Grönbeck, *J. Am. Chem. Soc.*, 2019, **141**, 8541–8549.
116 J. Nielsen, M. d'Avezac, J. Hetherington and M. Stamatakis, *J. Chem. Phys.*, 2013, **139**, 224706.
117 M. Andersen, C. Panosetti and K. Reuter, *Front. Chem.*, 2019, **7**, 202.
118 M. Pineda and M. Stamatakis, *J. Chem. Phys.*, 2022, **156**, 120902.
119 M. J. Hoffmann, S. Matera and K. Reuter, *Comput. Phys. Commun.*, 2014, **185**, 2138–2150.
120 L. Kunz, F. M. Kuhn and O. Deutschmann, *J. Chem. Phys.*, 2015, **143**, 044108.
121 M. Leetmaa and N. V. Skorodumova, *Comput. Phys. Commun.*, 2014, **185**, 2340–2349.
122 S. Shashkova and M. C. Leake, *Biosci. Rep.*, 2017, **37**, BSR20170031.
123 W. E. Moerner and D. P. Fromm, *Rev. Sci. Instrum.*, 2003, **74**, 3597–3619.
124 L. Edman, Z. Földes-Papp, S. Wennmalm and R. Rigler, *Chem. Phys.*, 1999, **247**, 11–22.
125 B. P. English, W. Min, A. M. van Oijen, K. T. Lee, G. Luo, H. Sun, B. J. Cherayil, S. C. Kou and X. S. Xie, *Nat. Chem. Biol.*, 2005, **2**, 87–94.
126 R. D. Smiley and G. G. Hammes, *Chem. Rev.*, 2006, **106**, 3080–3094.
127 K. Velonia, O. Flomenbom, D. Loos, S. Masuo, M. Cotlet, Y. Engelborghs, J. Hofkens, A. E. Rowan, J. Klafter, R. J. M. Nolte and F. C. de Schryver, *Angew. Chem., Int. Ed.*, 2005, **44**, 560–564.
128 T. Tachikawa, M. Fujitsuka and T. Majima, *J. Phys. Chem. C*, 2007, **111**, 5259–5275.
129 M. B. J. Roeffaers, B. F. Sels, H. Uji-i, F. C. De Schryver, P. A. Jacobs, D. E. De Vos and J. Hofkens, *Nature*, 2006, **439**, 572–575.
130 P. Chen, X. Zhou, N. M. Andoy, K.-S. Han, E. Choudhary, N. Zou, G. Chen and H. Shen, *Chem. Soc. Rev.*, 2014, **43**, 1107–1117.
131 P. Chen, X. Zhou, H. Shen, N. M. Andoy, E. Choudhary, K.-S. Han, G. Liu and W. Meng, *Chem. Soc. Rev.*, 2010, **39**, 4560.
132 B. Peters, *ACS Catal.*, 2022, **12**, 8038–8047.
133 S. R. Kulkarni, G. Lezcano, V. K. Velisoju, N. Realpe and P. Castaño, *ChemCatChem*, 2024, **16**, e202301720.
134 J. Cheng, P. Hu, P. Ellis, S. French, G. Kelly and C. M. Lok, *J. Phys. Chem. C*, 2008, **112**, 1308–1311.
135 H. Ooka, J. Huang and K. S. Exner, *Front. Energy Res.*, 2021, **9**, 654460.
136 G. Durin and C. Costentin, *ACS Catal.*, 2025, **15**, 2504–2514.
137 E. Pellegrino, A. Di Giuliano, N. Cancrini and K. Gallucci, *Chem. Eng. J.*, 2024, **488**, 150802.
138 R. Yang, Z. Bao and Y. Sun, *ACS Nanosci. Au*, 2023, **3**, 140–152.
139 R. Fan, P. Habibi, J. T. Padding and R. Hartkamp, *J. Chem. Phys.*, 2022, **156**, 084105.
140 G.-F. Wei and Z.-P. Liu, *Chem. Sci.*, 2015, **6**, 1485–1490.
141 D. Zhang, R. Wang, S. Luo and G. Wei, *Molecules*, 2024, **29**, 3549.

142 R. Ye, M. Zhao, X. Mao, Z. Wang, D. A. Garzón, H. Pu, Z. Zhao and P. Chen, *Nat. Commun.*, 2021, **12**, 4287.
143 B. Punia, S. Chaudhury and A. Kolomeisky, *J. Phys. Chem. Lett.*, 2023, **14**, 8227–8234.
144 A. Das and S. Chaudhury, *Chem. Phys. Lett.*, 2015, **641**, 193–198.
145 J. Kang, S. J. Park, J.-H. Kim, P. Chen and J. Sung, *Phys. Rev. Lett.*, 2021, **126**, 126001.
146 H. Xu, D. Cheng, Y. Gao and X. C. Zeng, *ACS Catal.*, 2018, **8**, 9702–9710.
147 Q. Liang, G. Brocks and A. Bieberle-Hütter, *J. Phys.: Energy*, 2021, **3**, 026001.
148 S. Neumann, T. Gutmann, G. Buntkowsky, S. Paul, G. Thiele, H. Sievers, M. Bäumer and S. Kunz, *J. Catal.*, 2019, **377**, 662–672.
149 M. P. C. van Etten, B. Zijlstra, E. J. M. Hensen and I. A. W. Filot, *ACS Catal.*, 2021, **11**, 8484–8492.
150 S. Chaudhury, D. Singh and A. B. Kolomeisky, *J. Phys. Chem. Lett.*, 2020, **11**, 2330–2335.
151 L. D. Marks, *Rep. Prog. Phys.*, 1994, **57**, 603–649.
152 C. Burda, X. Chen, R. Narayanan and M. A. El-Sayed, *Chem. Rev.*, 2005, **105**, 1025–1102.
153 S. Schauermann, J. Hoffmann, V. Johánek, J. Hartmann, J. Libuda and H.-J. Freund, *Angew. Chem., Int. Ed.*, 2002, **41**, 2532–2535.
154 V. Johánek, S. Schauermann, M. Laurin, J. Libuda and H. Freund, *Angew. Chem., Int. Ed.*, 2003, **42**, 3035–3038.
155 N. M. Andoy, X. Zhou, E. Choudhary, H. Shen, G. Liu and P. Chen, *J. Am. Chem. Soc.*, 2013, **135**, 1845–1852.
156 X. Mao, C. Liu, M. Hesari, N. Zou and P. Chen, *Nat. Chem.*, 2019, **11**, 687–694.
157 X. Mao and P. Chen, *Nat. Mater.*, 2021, **21**, 331–337.
158 B. Punia, S. Chaudhury and A. B. Kolomeisky, *Proc. Natl. Acad. Sci. U. S. A.*, 2022, **119**, e2115135119.
159 J.-P. Changeux and S. J. Edelstein, *Science*, 2005, **308**, 1424–1428.
160 J. Monod, J. Wyman and J.-P. Changeux, *J. Mol. Biol.*, 1965, **12**, 88–118.
161 Q. Cui and M. Karplus, *Protein Sci.*, 2008, **17**, 1295–1307.
162 M. O. Cichocka, Z. Liang, D. Feng, S. Back, S. Siahrostami, X. Wang, L. Samperisi, Y. Sun, H. Xu, N. Hedin, H. Zheng, X. Zou, H.-C. Zhou and Z. Huang, *J. Am. Chem. Soc.*, 2020, **142**, 15386–15395.
163 T. Sours, A. Patel, J. Nørskov, S. Siahrostami and A. Kulkarni, *J. Phys. Chem. Lett.*, 2020, **11**, 10029–10036.
164 G. Pajonk, *Appl. Catal., A*, 2000, **202**, 157–169.
165 M. Xiong, Z. Gao and Y. Qin, *ACS Catal.*, 2021, **11**, 3159–3172.
166 T. Tachikawa, S. Yamashita and T. Majima, *J. Am. Chem. Soc.*, 2011, **133**, 7197–7204.
167 B. Punia, S. Chaudhury and A. Kolomeisky, *J. Chem. Phys.*, 2024, **161**, 194107.
168 J. R. Canavan, J. A. Hopkins, B. L. Foley, O. A. Abdelrahman and P. J. Dauenhauer, *ACS Catal.*, 2025, **15**, 653–663.
169 X.-Y. Li, P. Ou, X. Duan, L. Ying, J. Meng, B. Zhu and Y. Gao, *JACS Au*, 2024, **4**, 1892–1900.
170 M. Xing, A.-D. Pathak, S. Sanyal, Q. Peng, X. Liu and X. Wen, *Appl. Surf. Sci.*, 2020, **509**, 144859.
171 P. Jangid, S. Chaudhury and A. Kolomeisky, *J. Phys. Chem. C*, 2025, **129**, 15606–15618.
172 P. Sabatier, La catalyse en chimie organique, Béranger, 1913.
173 M. Che, *Catal. Today*, 2013, **218–219**, 162–171.
174 A. J. Medford, A. Vojvodic, J. S. Hummelshøj, J. Voss, F. Abild-Pedersen, F. Studt, T. Bligaard, A. Nilsson and J. K. Nørskov, *J. Catal.*, 2015, **328**, 36–42.
175 M. D. Wodrich, B. Sawatlon, M. Busch and C. Corminboeuf, *Acc. Chem. Res.*, 2021, **54**, 1107–1117.
176 F. Tao, M. E. Grass, Y. Zhang, D. R. Butcher, J. R. Renzas, Z. Liu, J. Y. Chung, B. S. Mun, M. Salmeron and G. A. Somorjai, *Science*, 2008, **322**, 932–934.
177 P. Nolte, A. Stierle, N. Y. Jin-Phillipp, N. Kasper, T. U. Schulli and H. Dosch, *Science*, 2008, **321**, 1654–1658.
178 Z. W. Wang and R. E. Palmer, *Nanoscale*, 2012, **4**, 4947.
179 J. L. Rodrguez-López, J. M. Montejano-Carrizales, U. Pal, J. F. Sánchez-Ramrez, H. E. Troiani, D. Garca, M. Miki-Yoshida and M. José-Yacamán, *Phys. Rev. Lett.*, 2004, **92**, 196102.
180 M. A. Newton, C. Belver-Coldeira, A. Martínez-Arias and M. Fernández-García, *Nat. Mater.*, 2007, **6**, 528–532.
181 Y. Wang, S. Udyavara, M. Neurock and C. D. Frisbie, *Nano Lett.*, 2019, **19**, 6118–6123.
182 M. Yan, X. Pan, P. Wang, F. Chen, L. He, G. Jiang, J. Wang, J. Z. Liu, X. Xu, X. Liao, J. Yang and L. Mai, *Nano Lett.*, 2017, **17**, 4109–4115.
183 M. Shetty, M. A. Ardagh, Y. Pang, O. A. Abdelrahman and P. J. Dauenhauer, *ACS Catal.*, 2020, **10**, 12867–12880.
184 Z. Zhang, V. Du and Z. Lu, *Phys. Rev. E*, 2023, **107**, L012102.
185 M. Mavrikakis, B. Hammer and J. K. Nørskov, *Phys. Rev. Lett.*, 1998, **81**, 2819–2822.
186 A. Schlapka, M. Lischka, A. Gross, U. Käsberger and P. Jakob, *Phys. Rev. Lett.*, 2003, **91**, 016101.
187 A. Khorshidi, J. Violet, J. Hashemi and A. A. Peterson, *Nat. Catal.*, 2018, **1**, 263–268.
188 Y. Inoue, M. Matsukawa and K. Sato, *J. Am. Chem. Soc.*, 1989, **111**, 8965–8966.
189 S. R. Gathmann, M. A. Ardagh and P. J. Dauenhauer, *Chem. Catal.*, 2022, **2**, 140–163.
190 M. A. Murphy, S. R. Gathmann, R. Getman, L. Grabow, O. A. Abdelrahman and P. J. Dauenhauer, *Chem. Sci.*, 2024, **15**, 13872–13888.
191 J. R. Canavan, J. A. Hopkins, B. L. Foley, O. A. Abdelrahman and P. J. Dauenhauer, *ACS Catal.*, 2024, **15**, 653–663.
192 M. A. Ardagh, O. A. Abdelrahman and P. J. Dauenhauer, *ACS Catal.*, 2019, **9**, 6929–6937.
193 M. Shetty, A. Walton, S. R. Gathmann, M. A. Ardagh, J. Gopeesingh, J. Resasco, T. Birol, Q. Zhang, M. Tsapatsis, D. G. Vlachos, P. Christopher, C. D. Frisbie, O. A. Abdelrahman and P. J. Dauenhauer, *ACS Catal.*, 2020, **10**, 12666–12695.
194 C. D. Armstrong and A. R. Teixeira, *React. Chem. Eng.*, 2020, **5**, 2185–2203.

195 G. R. Wittreich, S. Liu, P. J. Dauenhauer and D. G. Vlachos, *Sci. Adv.*, 2022, **8**, eabl6576.
196 D. Huang, X. Ma, J. Xie, L. Pan, Q. Wang, T. Long, S. Zhao and Z. Wei, *Small*, 2025, **21**, e07002.
197 C. Luan, D. Escalera-López, U. Hagemann, A. Kostka, G. Laplanche, D. Wu, S. Cherevko and T. Li, *ACS Catal.*, 2024, **14**, 12704–12716.
198 C. A. Obasanjo, G. Gao, B. N. Khiarak, T. H. Pham, J. Crane and C.-T. Dinh, *Energy Fuels*, 2023, **37**, 13601–13623.
199 R. Casebolt DiDomenico, K. Levine, C. Bundschu, L. Reimanis, T. Arias and T. Hanrath, *ACS Catal.*, 2024, **14**, 785–796.
200 L. Xu, X. Ma, L. Wu, X. Tan, X. Song, Q. Zhu, C. Chen, Q. Qian, Z. Liu, X. Sun, S. Liu and B. Han, *Angew. Chem., Int. Ed.*, 2022, **61**, e202210375.
201 A. R. Woldu, P. Talebi, A. G. Yohannes, J. Xu, X.-D. Wu, S. Siahrostami, L. Hu and X.-C. Huang, *Angew. Chem., Int. Ed.*, 2023, **62**, e202301621.
202 X. Wu, X. Li, J. Lv, X. Lv, A. Wu, Z. Qi and H. B. Wu, *Small*, 2024, **20**, 2307637.
203 J. M. Gallagher, B. M. Roberts, S. Borsley and D. A. Leigh, *Chem*, 2024, **10**, 855–866.
204 B. Rocha, S. Paul and H. Vashisth, *Entropy*, 2020, **22**, 877.
205 R. G. Endres, *Sci. Rep.*, 2017, **7**, 14437.
206 U. Seifert, *Rep. Prog. Phys.*, 2012, **75**, 126001.
207 H. Qian, S. Kjelstrup, A. B. Kolomeisky and D. Bedeaux, *J. Phys.: Condens. Matter*, 2016, **28**, 153004.
208 J. Schnakenberg, *Rev. Mod. Phys.*, 1976, **48**, 571–585.
209 G. Sun and P. Sautet, *Acc. Chem. Res.*, 2021, **54**, 3841–3849.
210 T. Imaoka, T. Toyonaga, M. Morita, N. Haruta and K. Yamamoto, *Chem. Commun.*, 2019, **55**, 4753–4756.
211 J. Shi, S. Huang, F. Gygi and J. K. Whitmer, *J. Phys. Chem. A*, 2022, **126**, 3392–3400.
212 M. Chen, X. Zhou, C. Xiong, T. Yuan, W. Wang, Y. Zhao, Z. Xue, W. Guo, Q. Wang, H. Wang, Y. Li, H. Zhou and Y. Wu, *ACS Appl. Mater. Interfaces*, 2022, **14**, 21989–21995.
213 C. Wang, Q. Zhang, B. Yan, B. You, J. Zheng, L. Feng, C. Zhang, S. Jiang, W. Chen and S. He, *Nano-Micro Lett.*, 2023, **15**, 52.
214 V. Okatenko, A. Loiudice, M. A. Newton, D. C. Stoian, A. Blokhina, A. N. Chen, K. Rossi and R. Buonsanti, *J. Am. Chem. Soc.*, 2023, **145**, 5370–5383.
215 N. K. Razdan and A. Bhan, *Proc. Natl. Acad. Sci. U. S. A.*, 2021, **118**, e2019055118.
216 P. Poths and A. N. Alexandrova, *J. Phys. Chem. Lett.*, 2022, **13**, 4321–4334.
217 N. Razdan and A. Bhan, *J. Catal.*, 2021, **404**, 726–744.
218 J. Andrieux, U. Demirci and P. Miele, *Catal. Today*, 2011, **170**, 13–19.
219 S.-F. Wang, N. M. Umesh, S. Kameoka and B. Sriram, *ACS Appl. Nano Mater.*, 2024, **7**, 14372–14379.
220 J. A. Delgado, S. Castillón, D. Curulla-Ferré, C. Claver and C. Godard, *Catal. Commun.*, 2015, **71**, 88–92.
221 Z. Wang, P. Ma, K. Zheng, C. Wang, Y. Liu, H. Dai, C. Wang, H.-C. Hsi and J. Deng, *Appl. Catal., B*, 2020, **274**, 118963.
222 Y. Zhang, Y. Zhang, W. Guo, A. C. Johnston-Peck, Y. Hu, X. Song and W. D. Wei, *Energy Environ. Sci.*, 2020, **13**, 1501–1508.
223 T. E. Loman, Y. Ma, V. Ilin, S. Gowda, N. Korsbo, N. Yewale, C. Rackauckas and S. A. Isaacson, *PLoS Comput. Biol.*, 2023, **19**, 1–19.
224 J. Li, Y. Xi, Y. Qiao, Z. Zhao, J. Liu and F. Li, *ChemCatChem*, 2024, **16**, e202400120.
225 J. Wang, C.-Q. Lv, J.-H. Liu, R.-R. Ren and G.-C. Wang, *Int. J. Hydrogen Energy*, 2021, **46**, 1592–1604.
226 S. Ringe, N. G. Hörmann, H. Oberhofer and K. Reuter, *Chem. Rev.*, 2022, **122**, 10777–10820.
227 B. W. J. Chen, X. Zhang and J. Zhang, *Chem. Sci.*, 2023, **14**, 8338–8354.
228 V. Fung, G. Hu, P. Ganesh and B. G. Sumpter, *Nat. Commun.*, 2021, **12**, 88.
229 T. T. Duignan, *ACS Phys. Chem. Au*, 2024, **4**, 232–241.
230 G. Valadez Huerta, Y. Nanba and M. Koyama, *Surf. Interfaces*, 2025, **66**, 106542.
231 V. Gupta, K. Choudhary, B. DeCost, F. Tavazza, C. Campbell, W.-K. Liao, A. Choudhary and A. Agrawal, *npj Comput. Mater.*, 2024, **10**, 1.
232 T. Taniike, A. Fujiwara, S. Nakanowatari, F. Garca-Escobar and K. Takahashi, *Commun. Chem.*, 2024, **7**, 11.
233 Q. Li, Y. Ouyang, S. Lu, X. Bai, Y. Zhang, L. Shi, C. Ling and J. Wang, *Chem. Commun.*, 2020, **56**, 9937–9949.
234 C. Bozal-Ginesta, S. Pablo-Garca, C. Choi, A. Tarancón and A. Aspuru-Guzik, *Nat. Rev. Chem.*, 2025, **9**, 601–616.
235 W. Yang, T. T. Fidelis and W.-H. Sun, *ACS Omega*, 2020, **5**, 83–88.